Dielectric characterization of high-performance spaceflight materials

by

Nathan Alan Kleppe

A thesis submitted to the graduate faculty

in partial fulfillment of the requirements for the degree of

MASTER OF SCIENCE

Major: Material Science and Engineering

Program of Study Committee:
Nicola Bowler, Major Professor
Steve W. Martin
Sumit Chaudhary

Iowa State University

Ames, Iowa

2014

TABLE OF CONTENTS

LIST OF TABLES

LIST OF FIGURES

Page

NOMENCLATURE

BDS	Broadband Dielectric Spectrometer
ECTFE	Ethylene Chlorotrifluoroethylene
EVOH	Ethylene Vinyl Alcohol
FEP	Fluorinated Ethylene Propylene
FTIR	Fourier Transform Infrared Spectroscopy
HN	Havriliak-Negami
MWS	Maxwell-Wagner-Sillars
PAEK	Poly (Aryl Ether Ketone)
PEEK	Poly (Ether Ether Ketone)
PICA	Phenolic Impregnated Carbon Ablator
PFA	Perfluoroalkoxy
PPS	Polyphenylene Sulfide
PTFE	Polytetrafluoroethylene
PVDF	Polyvinylidene Difluoride
RF	Radio Frequency
SOP	Standard Operating Procedure
UHMWPE	Ultra-High Molecular Weight Polyethylene

ACKNOWLEDGEMENTS

I would like to express my thanks to those who have helped me with my research and in the writing of this thesis. First of all, I thank Dr. Nicola Bowler for her guidance and assistance throughout this process. Her support and encouragement has helped me through my graduate studies and realize my goals for the future. I would also like to thank Dr. Mark A. Nurge for his mentoring and support during this work and my time at NASA Kennedy Space Center. In addition, I would like thank my friends, family and the Material Science and Engineering faculty and staff for making these many years at Iowa State University an amazing experience.

Finally, thanks to the National Aeronautics and Space Administration for my acceptance into the NASA Space Technology Research Fellowship program and the funding for my research through the grant #NNX13AL81H.

ABSTRACT

As commercial space travel increases, the need for reliable structural health monitoring to predict possible weaknesses or failures of structural materials also increases. Monitoring of polymer-based materials may be achieved through the use of dielectric spectroscopy by comparing permittivity or conductivity measurements performed on a sample in use to that of a pristine sample. Changes in these measured values or of the relaxation frequencies, if present, can indicate chemical or physical changes occurring within the material and the possible need for maintenance/replacement. In this work, we established indicative trends that occur in the dielectric spectra during accelerated aging of various high-performance polymeric materials (EVOH, PEEK, PPS, and UHMWPE). Uses for these materials range from electrical insulation and protective coatings to windows and air- or space-craft parts that may be subject to environmental damage over long-term operation. Accelerated thermal aging and ultraviolet/water-spray cyclic aging were performed in order to investigate the degradation of the aforementioned material. The Havriliak-Negami model was used in the analysis of the measured dielectric spectra in order to obtain the characteristic fit parameters from which aging-related trends were identified. With reference to the literature and from measured FTIR spectra, observations were connected to the underlying mechanisms causing the dielectric relaxations.

CHAPTER 1. INTRODUCTION

1.1 Research Motivation

Spacecraft materials are subjected to a wide range of conditions both while in-service and not in-service which can decrease the material's ability to perform its intended function. Many of the materials used for the launch of a spacecraft can be affected by the uptake of water from the air when subjected to high humidity in the environment, the sun's radiation, by accidental damage during maintenance or while in-service, causing the material to wear out before its intended life span or fail prematurely. These issues can cause high maintenance costs and, in the extreme cases, loss of life and property from the failed detection of flaws within the material. Since many of the current launch sites for space bound companies within the United States are located in warm, high humidity environments, the detection and prevention of a material's weakening is of high importance.

Dielectric spectroscopy is expanding in popularity as a technique used to measure a material's properties nondestructively but there are still gaps in knowledge on how a material will respond, from a dielectric standpoint, after being degraded. The analysis of these materials is useful for the understanding of their complex permittivities and their response to the changes of their surroundings. Using this understanding combined with the use of capacitive sensors to obtain the dielectric measurements, the materials can be monitored for unwanted changes which occur over time.

1.2 Background

1.2.1 Dielectric Spectroscopy

Dielectric spectroscopy is the measurement of a material's dielectric properties as a function of frequency or temperature. Within the frequency range used, which varies based on the application, the relevant relaxation modes are shown as peaks in the imaginary permittivity (ε''), or loss factor, as a function of frequency. A relaxation is also indicated by a sudden decrease in the real permittivity (ε') around the corresponding relaxation frequency (Figure 1). These relaxation modes represent the inability of one or more polarization mechanisms in the material, above their relaxation frequencies, to re-align quickly enough to the applied electric field and contribute to its polarization.

The four fundamental polarization mechanisms are interfacial, orientational, ionic and electronic. Each one involves the preferential alignment of an electric dipole within the direction of the applied electric field but differ by the scale at which these alignments occur. The larger the scale, the slower the mechanism is at aligning to the applied field; this means a lower frequency is needed to cause the polarization mechanism to be lost. Interfacial polarization typically occurs along grain boundaries and interfaces which require a low frequency to overcome the mechanism's ability to respond. Whereas electronic polarization is primarily the harmonic oscillation between the valence electrons and the nucleus of the atoms, which naturally oscillate at a high frequency (varies between atoms of different sizes). This requires a very high frequency in order to overcome the binding energy between the electron and the nucleus and as a result, it is the last polarization mechanism to be lost as frequency increases.
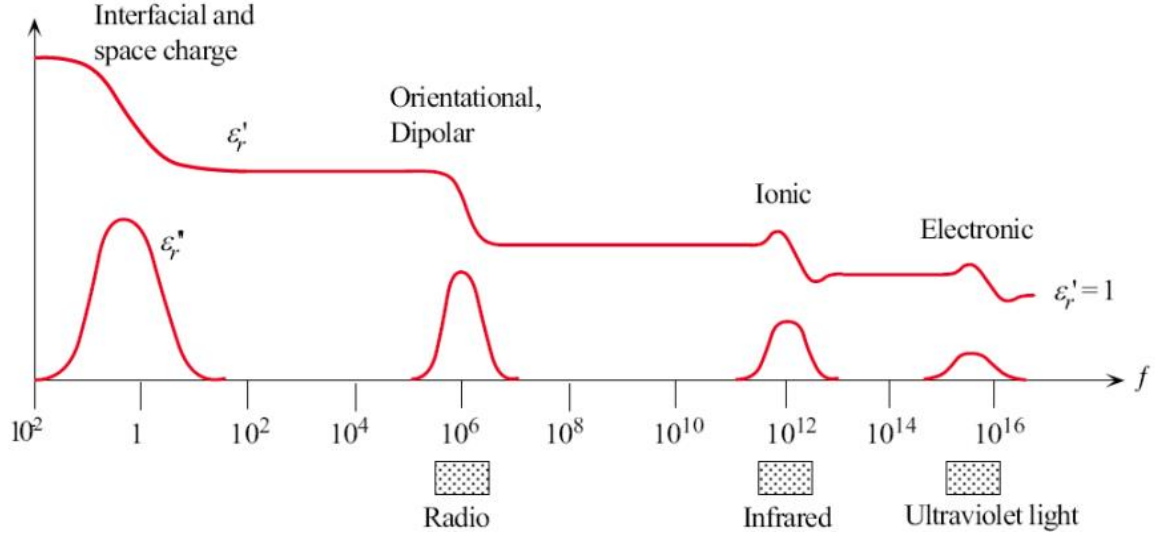
Figure 1. Schematic diagram of the correlation between the real and imaginary permittivities of a hypothetical material as a function of frequency, when interfacial, orientational, ionic, and electronic polarization mechanisms are present (Figure 7.15 in [1]).

The complex capacitances of the samples were measured using a Novocontrol dielectric spectrometer through the use of a parallel plate capacitor. Complex permittivities of the samples are obtained by the rearrangement of Equation 1:

$$C = \frac{\varepsilon A}{d}$$

(1)

where, C is capacitance, ε is permittivity of the medium between the electrodes, A is the area of one of the (identical) electrodes, and d is the distance between the electrodes (sample thickness). The real and imaginary permittivity values are related to the complex permittivity (ε) by Equation 2:

$$\varepsilon = \varepsilon' - j\varepsilon''$$

(2)

where, ε' is the real permittivity and ε'' is the imaginary permittivity.

From these relationships the Novocontrol system analysis software (WinDeta) calculates the components of the complex permittivity and allows for plotting in various desired formats. Data analysis was performed using the corresponding WinFit software and

the data files were produced in WinDeta.

Another way to convey dielectric measurements other than the standard permittivity verses frequency arrangement is by plotting them as ε'' verses ε' (note: ε'' is actually plotted as $-\varepsilon''$), also known as a Cole-Cole diagram (Figure 2). From these diagrams additional information can be revealed about the material; for example, additional relaxations which are difficult to observe in the ε'' verses frequency plots, the presence of low frequency conductivity, and information about the characteristic fit parameters. The diagrams show that under the ideal conditions the characteristic relaxation frequency occurs at a maximum in $|\varepsilon''|$ (the peak of (a)) and the relaxation time is related to its frequency by Equation 4:

$$f = \frac{1}{2\pi\tau} \tag{4}$$

where, f is frequency and τ is the relaxation time. This relaxation time is also related to the characteristic fit parameters β and $\Delta\varepsilon$ by the relationship shown in Equation 5:

$$\beta\tau = \Delta\varepsilon = \varepsilon_s - \varepsilon_\infty \tag{5}$$

where, ε_s is the static, low frequency permittivity and ε_∞ is the high frequency permittivity.

(a)   **(b)**
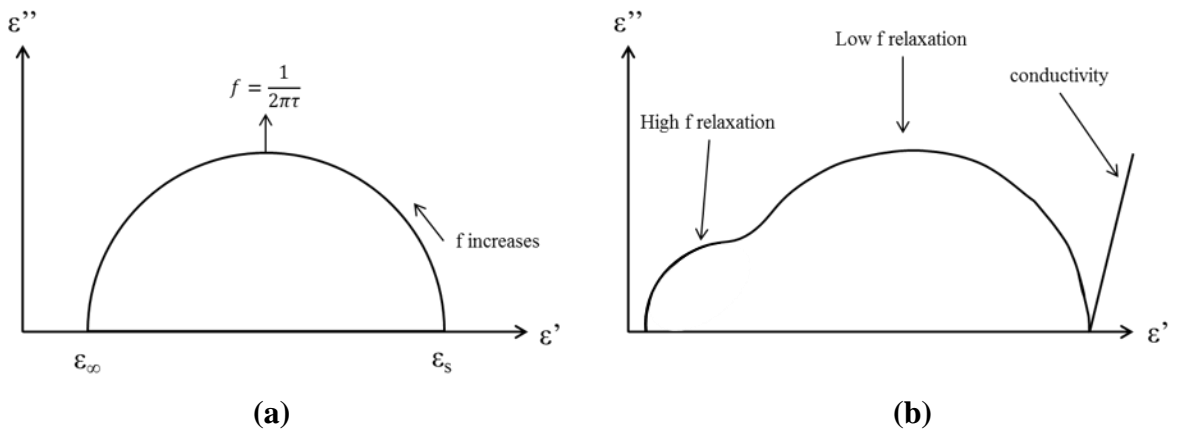
Figure 2. Example Cole-Cole plots of an idealized dielectric with one relaxation (a) and a material with two relaxations with low frequency conductivity (b).

The imaginary component of the complex permittivity can be expressed as the sum of a power law conductivity term and the Havriliak-Negami model [2], as shown in Equation 3:

$$\varepsilon''_{HN} = \frac{\sigma}{\varepsilon_0 \omega^S} + Im\left[\frac{\Delta\varepsilon}{(1+(j\omega\tau)^\alpha)^\beta}\right] \tag{3}$$

where, σ is the conductivity, ε_o is the permittivity of free space, ω is the angular frequency, τ is the characteristic relaxation time, α and β are the characteristic relaxation shape parameters ($\alpha > 0$ and $\beta \leq 1$, but β can be greater than 1 if $\alpha\beta \leq 1$), and the power S is due to conductivity and electrode polarization effects ($S \leq 1$) [2].

The relaxation mechanisms which occur within the material and their corresponding fit parameters can be used to monitor materials for changes in water content, radiation and thermal damage, and porosity because the relative permittivity of air is low compared to most materials (1.0005 at room temperature) and water has a higher permittivity than many materials (about 80 at room temperature) [1]. When a dry, defect free material is measured, a consistent signal should be obtained but as the amount of the aforementioned changes occur, the signal will also reflect the relative amounts based on the distortion of the original signal. Predictable distortions also occur as the temperature changes because of the change in thermal energy present in the material which causes the relaxation frequencies to shift accordingly to the difference in thermal energy. These shifts cause the relative permittivity of a material to change with temperature.

The Havriliak-Negami model was used in the analysis of the materials in order to examine relaxation frequencies characteristic shape parameters, the amount of conduction present, and how they change as a result of the accelerated aging. A low frequency relaxation process and conductivity was performed by using the least squares mean deviation fitting process in Novocontrol's WinFit software [3] to determine the parameters that appear in

Equation 3. The orders in which parameters are chosen to be optimized are subject to the user's discretion and can lead to varying results based on the order chosen.

1.2.2 Spaceflight Materials

The extreme conditions materials can be exposed to during spaceflight can extend from a wide range of temperatures (i.e. from around -156 °C in the shade to 250 °C in the sunlight while in space [4]), high stresses due to the excessive gravitational forces (the former space shuttles would experience up to three times normal gravitational force [4]), exposure to atmospheric weathering (ultraviolet, moisture and thermal exposures), and many others. In order to ensure these structures perform as they are intended to, a wide variety of high-performance materials are used in their construction. To ensure this wide variety was covered, 27 materials were selected for testing, as listed in Table 1.

Table 1. Full group of materials examined. The materials discussed in detail in this thesis are indicated by (*).

Aerogel (Pyrogel)	AVCOAT	Carbon Fabric 57-3K
Delrin	ECTFE	EVOH*
FEP	Garolite	Impact-Resistant Polycarbonate
Kapton	Kevlar K29-745	Kevlar K49-352
Kevlar K49-353	Kevlar K129	Kevlar K159-779
PEEK*	PFA	PICA
PPS*	PTFE	PVDF
Tefzel	UHMWPE*	ULTEM
Upilex	Vespel	Wear-Resistant Nylon

In this thesis four materials have been chosen for detailed discussion due to their noticeable changes in dielectric response after aging, Ethylene Vinyl Alcohol (EVOH), Poly (ether ether ketone) (PEEK), Polyphenylene Sulfide (PPS) and Ultra-High Molecular Weight Polyethylene (UHMWPE). These materials contained clear trends and had distinctive results.

1.3 Thesis Organization

This thesis addresses the results of accelerated weathering and thermal aging experiments performed on four materials of interest, EVOH, PEEK, PPS, and UHMWPE and how those results could be used as a reference in development of nondestructive evaluation methods for inspection of spaceflight materials. Chapter 1 includes a general introduction to the thesis and the fundamentals of dielectric spectroscopy. Chapter 2 contains a literature review of relevant published information for the materials being discussed. Chapter 3 addresses the methodology used to carry out the dielectric characterization and the aging processes. Chapters 4 and 5 include the results and a discussion of their significance. Chapter 6 addresses the general conclusions and summarizes key findings obtained from this research. The remaining section contains the references used in this work.

CHAPTER 2. LITERATURE REVIEW

2.1 Ethylene Vinyl Alcohol

Ethylene Vinyl Alcohol (EVOH) is a copolymer of ethylene and vinyl alcohol (Figure 3) with increasing uses in areas were gas permeation barriers are needed, where n was approximately 40 for this work. This is because of its tendency to readily oxidize when excess oxygen is present [5]. From a dielectric standpoint, information is scarce on how its permittivity changes with respect to frequency. Most of the literature is centered on the oxidation behaviors [5, 6]. It has been suggested though that the β-relaxation is likely due to either the local relaxation of crystalline regions or the movement of hydroxyl groups which may interact with each other from one vinyl alcohol groups to another, inhibiting chain motion [6].
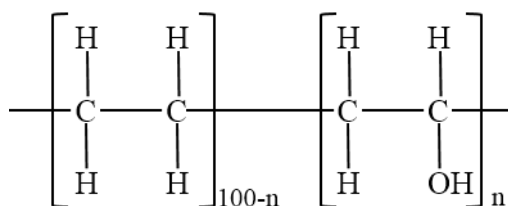
Figure 3. Chemical structure of ethylene vinyl alcohol (EVOH).

Aging of EVOH in the presence of a radiation source (i.e gamma radiation) has been shown to cause degradation through the formation of carbonyl, hydroperoxide and hydroxyl groups when in the presence of oxygen. This is likely due to the preferential targeting of the H-C-OH sites by oxygen and has been verified through FTIR analysis. Absorption peaks around 3400 and 1720 cm^{-1} were observed which correspond to the absorption of alcohol and carbonyl species, respectively [5].

2.2 Poly (ether ether ketone)

Poly (ether ether ketone) (PEEK) is a semi-crystalline aromatic polyether thermoplastic designed for high temperature use under the name "Victrex" [7]. Repeat units consist of a carbon-oxygen chain with aromatic rings as shown in Figure 4. This type of polymer is part of the polyaryletherketone (PAEK) class which is characterized by benzene rings attached to oxygen and ketone groups [8]. The polymer has a relatively high melting point of around 340 °C due to these aromatic rings [7]. Because of its high thermal, chemical and radiation resistance it has become a popular material for aerospace use.
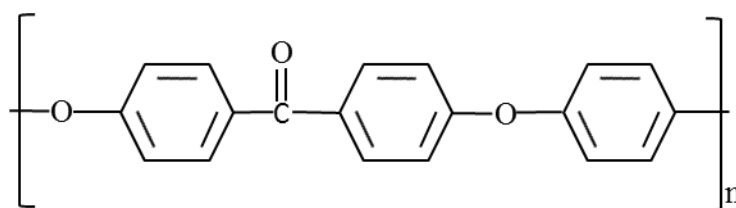
Figure 4. Chemical structure of poly (ether ether ketone) (PEEK).

At room temperature PEEK has a dielectric constant around 3.5 and a primary (α-) relaxation (for this frequency range) which occurs above 100 kHz – 3 MHz. Typically Maxwell-Wagner-Sillars (MWS) effects are observed within this frequency range (γ in Figure 5), which is an interfacial relaxation present in heterogeneous materials when subjected to an electric field [9, 10, 11, 12]. These heterogeneous sites include amorphous/crystalline regions, impurities or chemicals remaining from processing (i.e plasticizers or catalysts) whose permittivity or conductivity values are different from those of the main phase [10].

At high frequency, below the glass-transition temperature (143 °C [7]), a broad relaxation occurs which is characterized by the localized non-cooperative motions of the

chain fragments, primarily the resonance of the aromatic rings [12]. This process is the β-relaxation and is associated with the initial movement of the glass-transition relaxation (α) which occurs above 143 °C [9].
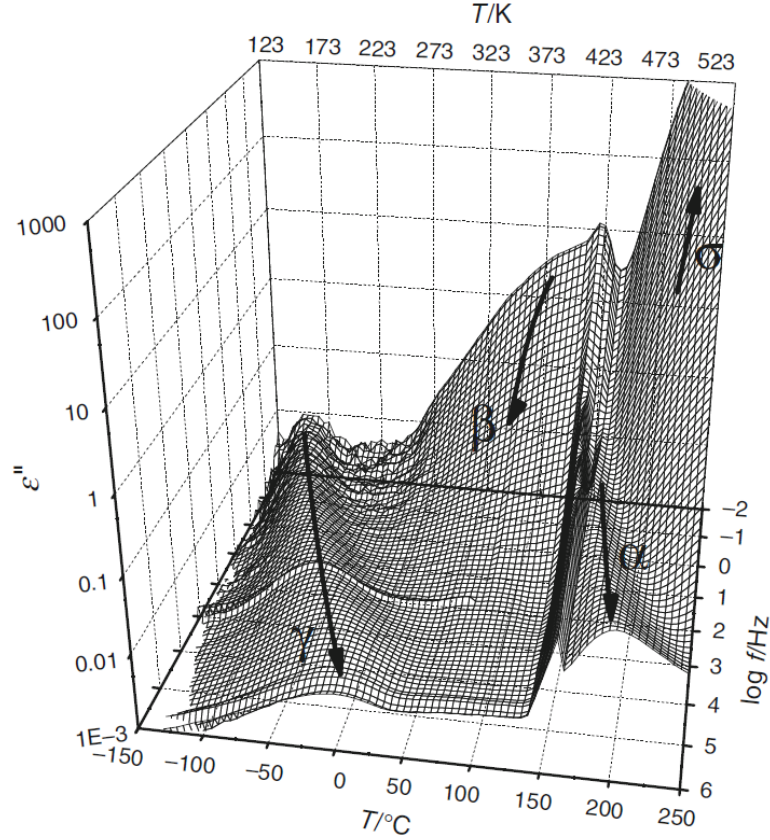
Figure 5. Temperature and frequency profile of ε'' on PEEK (Figure 6 of [12]).

With increasing radiation exposure or thermal aging, the frequencies of the sub-glass-transition relaxations (β and γ) have been observed to decrease [9, 10]. These decreases are the result of increased cross-linking (observed by an increase in C-C bonding within the IR spectrum) and oxidation in the presence of oxygen. The value of real permittivity was observed to increase with aging, however, due to the increase of dipoles and ions present after aging [11]. It will be seen in section 4.2.3 that our findings were consistent with this observation.

2.3 Polyphenylene Sulfide

Polyphenylene Sulfide (PPS) is a high temperature thermoplastic which is usually characterized as a semi-crystalline polymer with a high degree of crystallinity, high thermal resistance, mechanical properties and a high melting point (about 280 °C depending on the degree of crystallinity) [13, 14, 15, 16]. These properties make PPS a great material for electrical uses, composites, and insulation. In addition to its insulative properties, the material can become conductive when heavily oxidized or doped with electron acceptors [14, 15]. A small repeat unit consisting of an aromatic ring bonded to a sulfur atom comprises the polymer structure (Figure 6).
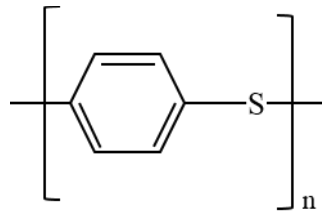
Figure 6. Chemical structure for polyphenylene sulfide (PPS).

From a dielectric standpoint, PPS has a weak dependence between ε' and frequency. Three relaxations are typically present below the glass transition temperature, an interfacial relaxation between the crystalline and amorphous phases (MWS effects), a relaxation due to the rotation of the aromatic ring, and one due to chain motion [13, 15]. An example of ε'' can be seen in Figure 7.

Due to its relatively stiff chains, when heated near or above its glass transition temperature (approximately 90 °C) in the presence of oxygen, the material will heavily cross-link which causes an increase in ε''; however, heating the polymer above its melting point causes significant oxidation of the aromatic rings and sulfur [14]. Upon cooling, the material

also has a high tendency to crystalize.
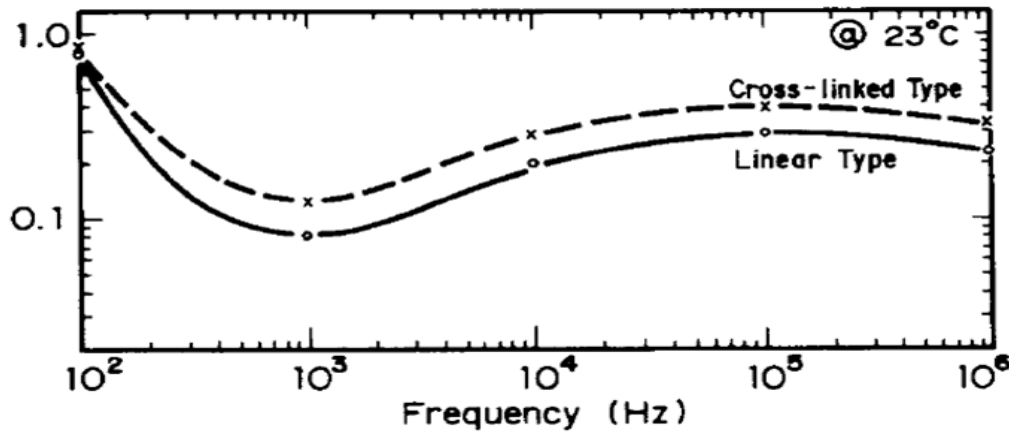
Figure 7. An example of the permittivity of linear and cross-linked PPS (Figure 6 from [16]).

2.4 Ultra-High Molecular Weight Polyethylene

Ultra-High Molecular Weight Polyethylene (UHMWPE) is a polymer consisting of a carbon chain with hydrogen side groups with an exceptionally high molecular weight, as seen in Figure 8. The dielectric constant of UHMWPE at 1 kHz is roughly 2.3 [17, 18]. This value has been shown to increase with radiation exposure (Figure 9). The material can be extensively damaged by ionizing radiation, especially when in the presence of oxygen. This is caused by the formation of free radicals and chain fragments due to the breaking of bonds which create localized charged sites [17]. These defect sites can interact with other chains to cause cross-linking and further oxidation. As the amount of cross-linking increases, interfacial polarization increases between the crystalline and amorphous regions. FTIR analysis of these interactions are shown in Figure 10 with the peaks of interest outlined in red (from left to right: hydroxyl, carbonyl and C-C groups) [17].
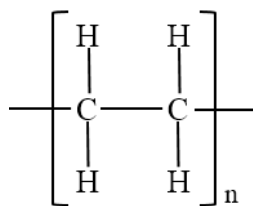
Figure 8. Chemical structure for ultra-high molecular weight polyethylene (UHMWPE).
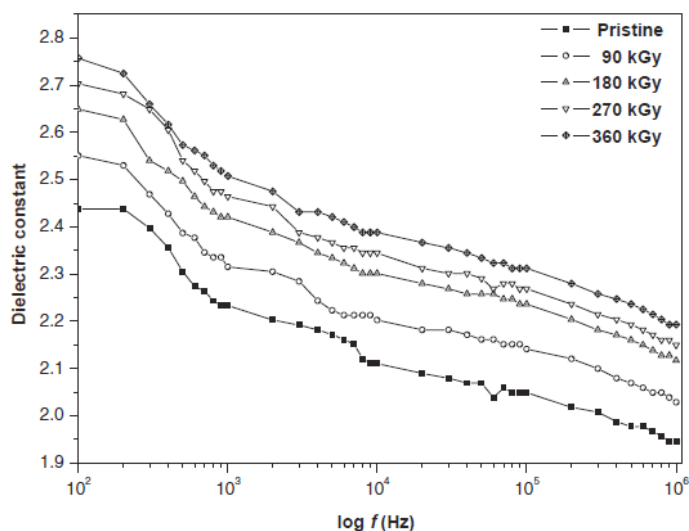
Figure 9. The real permittivity verses log (frequency) of a UHMWPE film with increasing radiation exposure (Figure 7 from [17]).
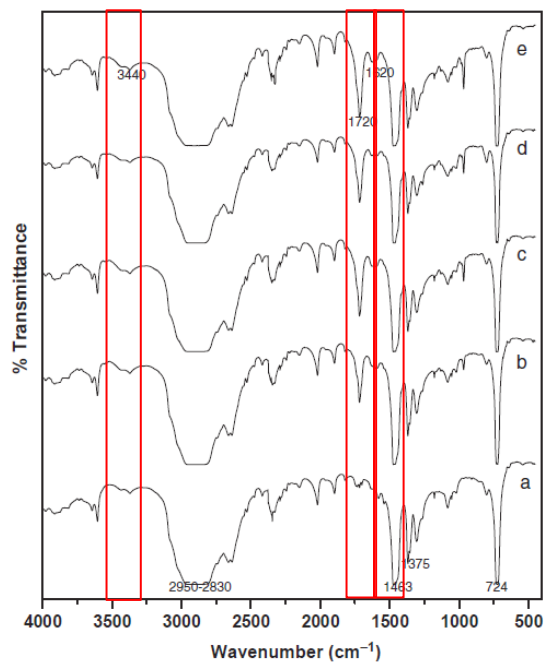
Figure 10. FTIR spectrum of pristine UHMWPE (a) with increasing radiation exposure (b-e) (Figure 1 of [17]).

CHAPTER 3. METHODOLOGY

3.1 Spectroscopic Baseline Measurements

Low and high frequency dielectric measurements were performed on the materials using the Novocontrol Broadband Dielectric Spectrometer (BDS) as outlined in the user manual [3]. Every day before testing began calibrations were performed in order to minimize any accidental equipment adjustments that possibly occurred during its previous use (loosening of wires or screws, misalignments of plates, etc.). These calibrations, which vary with the type of analyzer being used, are built into the WinDeta software and on-screen prompts guide the user through each necessary step. Following the calibrations a Teflon standard was tested to verify the correct values were being obtained.

The Alpha AN Analyzer for the Novocontrol system, which acts as a parallel-plate capacitor, was used for the low frequency measurements (10 mHz to 10 MHz). 20-mm-diameter disks of each material were punched from the as-received sheets and 10 thickness measurements were performed across each sample to obtain an average thickness. The average thickness, a one picofarad cell-stray (the user manual recommends the use of this value), sample name, and the diameter of the sample were input into the WinDeta software for each sample and edge effect compensation was also turned on. Before beginning each test, the samples were placed between two auxiliary electrodes, placed into the ZGS sample holder, Figure 11(a), and lowered into the cryostat tube, Figure 11(b), to minimize any external electrical interference.

(a)   (b)
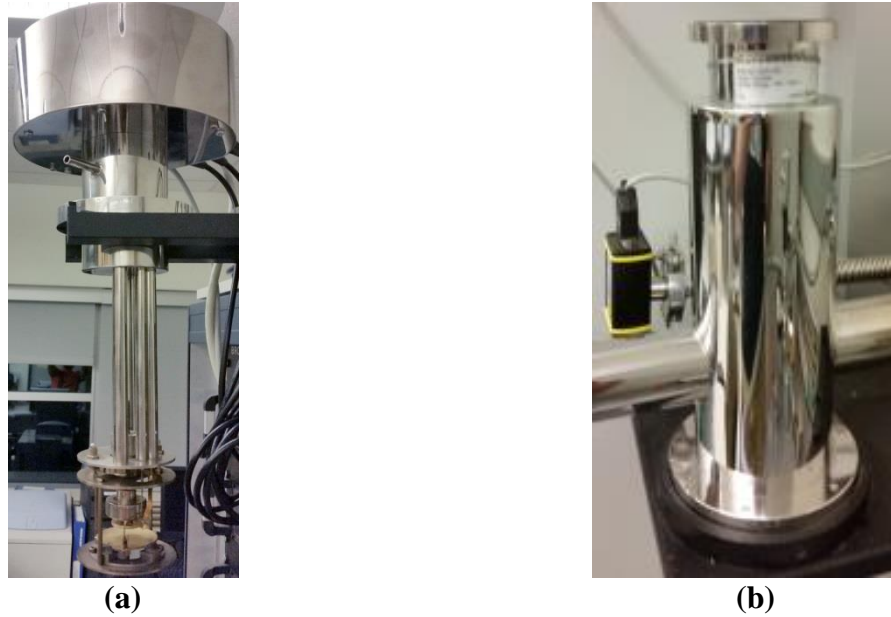
Figure 11. The ZGS sample holder (a) used for low frequency measurements, which was placed into the cryostat (b) during testing.

An Agilent 4991 Radio Frequency (RF) Impedance Analyzer was used for the high-frequency measurements (1 MHz to 3 GHz), seen in Figure 12(a). Seven-millimeter-diameter disks of each material were used with the BDS 2100 7 mm RF sample cell. The same sample inputs as described in the previous paragraph were used here, with the exception of a zero picofarad cell-stray and no edge effect compensation was necessary as these values are included by the software during the calibration process. After the sample cell was assembled and attached to the RF extension line, Figure 12(b), it was lowered into the cryostat tube and testing can begin.
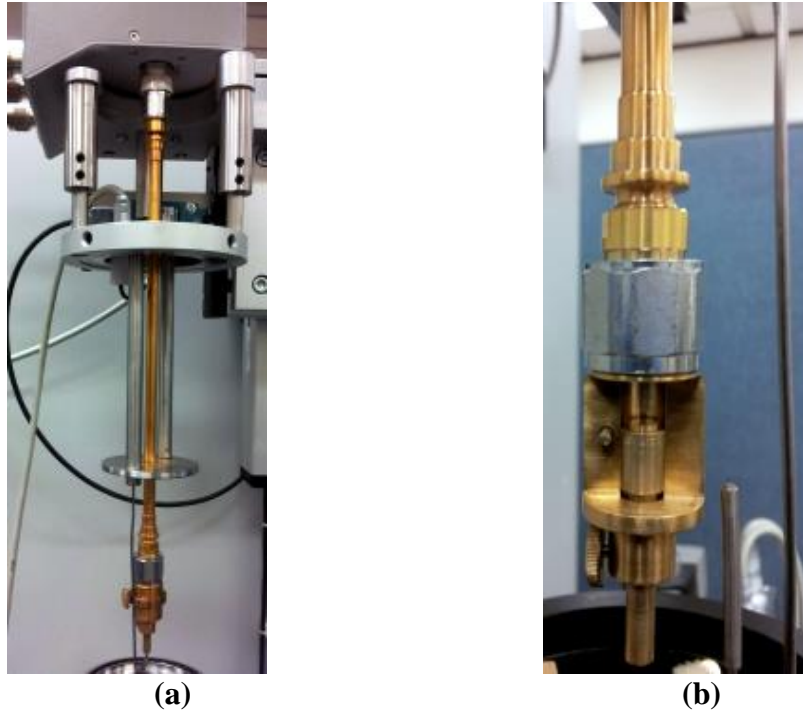
Figure 12. The Agilent 4991 (RF) Impedance Analyzer and extension line (a) with a close-up on the BDS 2100 7 mm RF sample cell attached to the extension line (b).

After the measurements were concluded, the data was exported into WinFit for analysis. The Havriliak-Negami function was used by the software to determine the fit characteristics and parameters, as described in Section 1.2.1 above, in order to examine if any spectral changes occurred after accelerated aging.

3.2 Weathering Experiments

3.2.1 Material Testing

The materials were tested using the Q-SUN Xe-3 Xenon Test Chamber following the standard, ASTM G155, "Standard Practice for Operating the Xenon Arc Light Apparatus for Exposure of Non-Metallic Materials" [19]. This standard tries to recreate the property changes associated with weathering effects which occur when non-metallic materials are

exposed to sunlight, moisture, and heat. Exposure conditions are listed in Table 2.

Table 2: Weathering exposure conditions as suggested in Cycle 1 of Table X3.1 in [19].

Filter Used:	Daylight
Irradiance:	0.35 W/(m^2 * nm)
Wavelength:	340 nm
Exposure Cycle:	102 minutes of light at 63 ± 2.5 °C black panel temperature
	18 minutes of light and water spray (air temperature not controlled)

A portion of each material, measuring 22 cm long by 5 cm wide (8-11/16" by 2"), were placed in sample holders and held in place by a circular ring, seen in Figure 13. The rings secured the material in place without inducing any unnecessary stress which would alter the end effects. The samples were placed into the test chamber for six weeks of continuous exposure and were only interrupted after a week of exposure in order to remove a one inch long section of the material to monitor the degradation process. A normal week's worth of cycles would end after the light and water spray portion of the cycle but due to the excess moisture altering the material's dielectric response, samples were removed before the final light and water exposure. Before beginning a new week of exposure, the sample holders were repositioned within the chamber to minimize any location variations in irradiance or moisture levels in the test chamber.

Figure 13. Q-SUN Xe-3 Xenon Test Chamber containing all 27 materials in their sample holders prior to the six weeks of weathering.

Once removed from the test chamber, following the same procedure as outlined in Section 3.1 above, disks were punched from the material (7 mm in diameter for high frequency and 20 mm in diameter for low-frequency dielectric measurements) and thickness measurements were taken before testing their dielectric spectra.

3.2.2 FTIR Characterization

To characterize the chemical changes which occur within the polymers as a result of the weathering experiment, FTIR measurements were performed on pristine samples of each material using the Shimadzu IRAffinity-1 Fourier Transform Infrared Spectrophotometer, seen in Figure 14, to obtain a pristine spectrum. Spectra were measured using the transmission mode from 4000 to 400 cm^{-1} as outline by Iowa State University's Department of Materials Science and Engineering standard operating procedure (SOP) for the Shimadzu FTIR [20].

Figure 14. The Shimadzu IRAffinity-1 FTIR used to examine the chemical changes caused by the accelerated weathering.

The material which remained from the six week exposure sample, after samples were prepared for dielectric spectroscopy, was used for FTIR measurements to examine the chemical changes which occurred as a result of the weathering process. The same procedure used to obtain the pristine FTIR spectra was used and the measured spectra were compared to their pristine counterparts to determine the changes in chemical bonding which occurred.

3.3 Thermal Degradation Experiments

Using a Lab-Line Imperial V, Model 3488M oven, each material was aged following a modified version of ASTM D3045, "Standard Practice for Heat Aging of Plastics Without Load," [21]. The temperatures used were higher than suggested within the standard in order to decrease the needed aging time. This was done because the standard calls for temperatures within the normal working range of the polymer for an aging time of up to 49 weeks. By using an aging temperature above their normal working range, the aging time could be lowered to one week. Three exposure times were chosen; one hour, one day and one week, at

a temperature close to the material's melting points (100 °C for EVOH [22] and UHMWPE [18], 200 °C for PPS [23] and 300 °C for PEEK [7]) to monitor if changes in permittivity were observed as quickly as physical changes were observed (typically physical changes were seen after one hour of aging).

Following the exposure for a given time interval, a 20-mm-diameter sample of each material was removed from the oven and the thickness was measured to account for any changes due to the aging process. Using the procedure outlined in Section 3.1.1, the dielectric spectra were then tested and compared to their counterparts for analysis.

CHAPTER 4. EXPERIMENTAL RESULTS

Within the dielectric measurements there were many sources of uncertainty which could have influenced the results. One source was from thickness measurements because a ten point average was taken from various locations around the sample but in some cases, the variation between values was as high as 10%. This variance, along with truncations within the WinDeta and WinFit programs (WinDeta rounded thickness measurements to 0.0001 mm and WinFit rounded to 0.001 mm), could have caused the permittivity values to be slightly higher or lower than what they should have been. These variations could explain the differences between the ε' values of the pristine measurements. Another source of uncertainty was in the accuracy of the analyzers. The low frequency analyzer inherently starts to lose accuracy above 1 MHz (up to its maximum frequency of 10 MHz) and the high frequency analyzer starts to lose accuracy above 1 GHz (up to the 3 GHz used). If the proper care was taken during the calibrations and setup of the sample holder, these accuracies could be improved; however, this was difficult to guarantee for every sample tested due to the handling of the samples and equipment. If the samples and electrodes or the wires and fasteners on the sample holder have a different amount of contact between each other compared to calibrations or previous tests, the capacitance could vary, changing the permittivity values since the electrode diameter and sample thickness should remain roughly the same.

4.1 Ethylene Vinyl Alcohol

4.1.1 Pristine Dielectric Measurements

Dielectric measurements conducted in the frequency range of 10 mHz to roughly 1 GHz at ambient temperature on pristine samples of EVOH revealed a relaxation around 160 kHz for each sample of EVOH tested (Figure 15). Low frequency conductivity (below 1 Hz) was also observed in these measurements, as seen by the increase in ε' and ε'' within this frequency range (Figure 15(a) and (b), respectively) and the sharp increase at low frequency present in the Cole-Cole plot, Figure 15(c). At 1 kHz the average ε' for the pristine samples was 5.0 ± 0.5 which corresponds to a variance between samples of approximately 9%.

Figure 16 shows an example fit for EVOH and the likely components which comprise the dielectric response within the frequency range being examined. The major components of the spectrum consist of two relaxations, a likely β-relaxation and a MWS relaxation, and an influence from low frequency conductivity. Fit parameters obtained from the HN model are shown in Table 3.
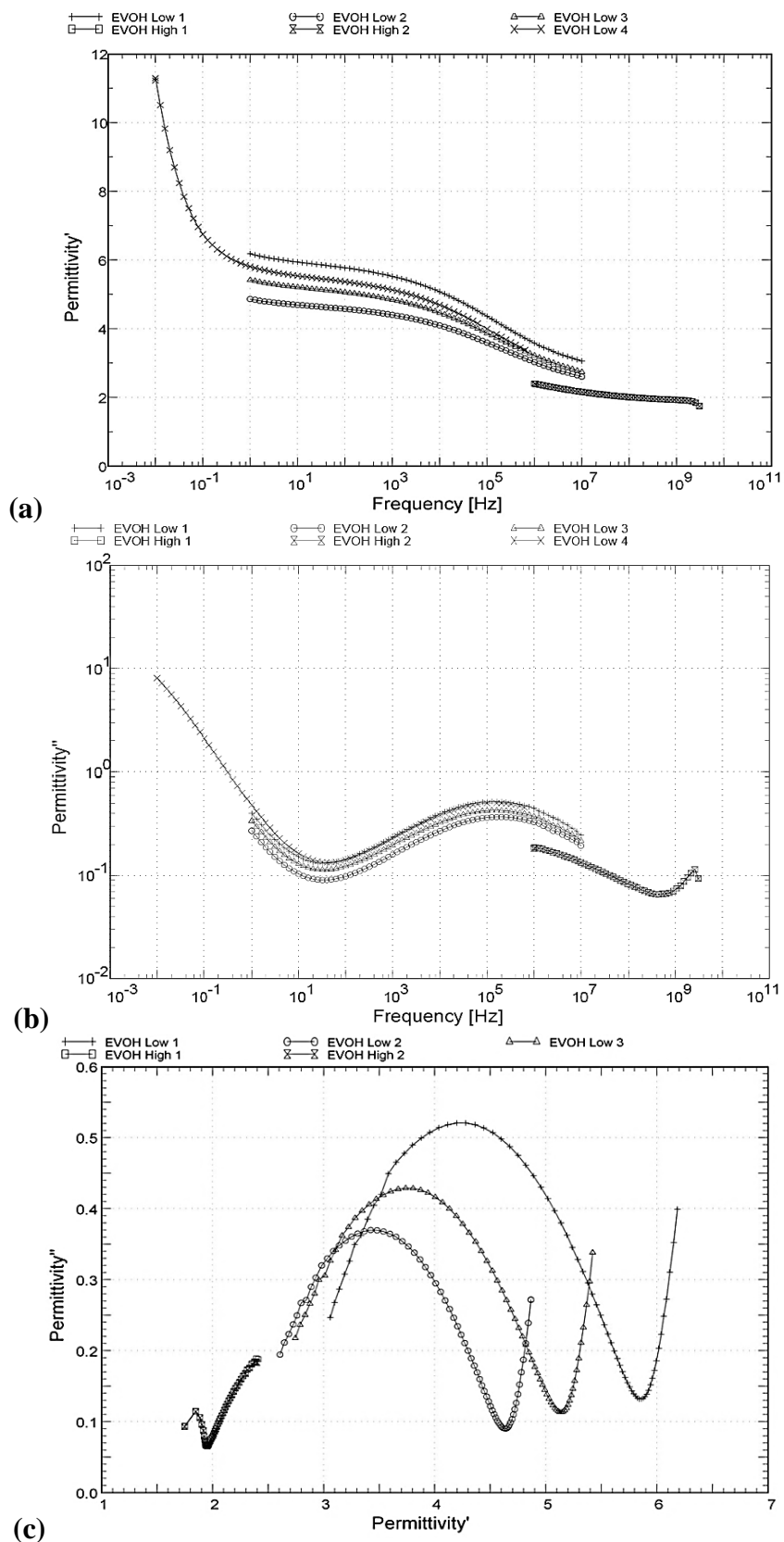
Figure 15. Pristine EVOH dielectric measurements plotted as ε' versus log (frequency) (a), log (ε'') versus log (frequency) (b) and a Cole-Cole representation (c).
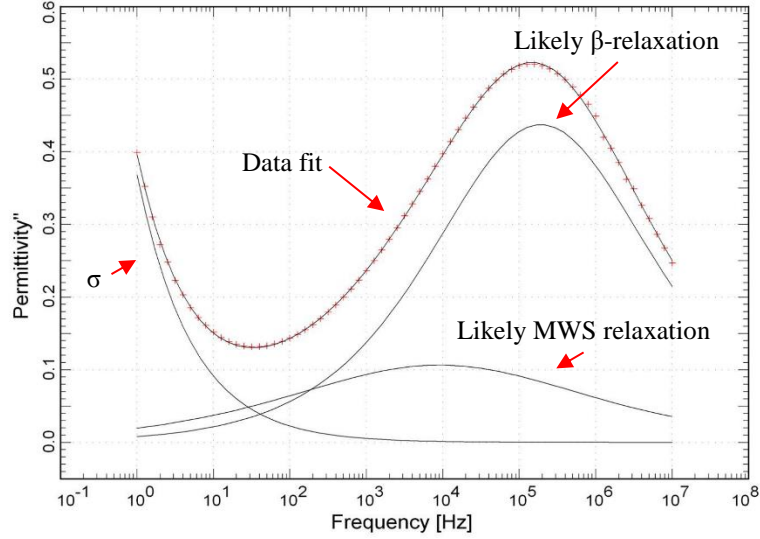
Figure 16. The data fit produced by the Havriliak-Negami function in WinFit on the pristine EVOH sample Low 1 plotted as ε'' verses log (frequency).

Table 3. Low frequency fit parameters for pristine EVOH.

Sample	σ (x10^{-13} S/m)	S	$\Delta\varepsilon$	τ (s)	α	β	ε_{∞}
Low 1	1.07	0.61	2.49	8.35x10^{-7}	0.43	1.00	2.23
			0.83	1.77x10^{-5}	0.32	1.00	
Low 2	0.60	0.63	2.05	7.67x10^{-7}	0.41	1.00	2.24
			0.38	8.02x10^{-5}	0.28	0.98	
Low 3	0.87	0.64	2.44	9.12x10^{-7}	0.40	1.00	2.34
			0.42	1.73x10^{-4}	0.28	1.00	

4.1.2 Weathering Experiment

4.1.2.1 Dielectric Measurements

After six weeks of weathering, no significant trends were observed within the dielectric spectra (shown in Figure 18). Every week changes were observed within the spectra but these changes did not develop into any distinct trends. The ε' values decreased after the first week and increased until week three but decreased after week four. From here the values again increased until completion of the weathering experiments. The imaginary permittivity (ε'') varied between the weeks with no particular order. Weeks 1-4 were outside

one standard deviation from the average pristine values at 1 kHz and can be considered a significant change but weeks 5 and 6 were near the mean values.

Generally speaking, the β-relaxation was not altered much as a result of the accelerated weathering but the MWS relaxation was found to shift to lower frequency with increased weathering (as shown by the fit parameters in Table 4). No other trends were observed within the fit parameters. The samples labeled as "retest" were reexamined due to being removed during the water cycle which influenced the results as described in Chapter 3.

The EVOH samples during the six weeks did become extremely brittle and shrank over time (shown in Figure 17). After week two, care had to be taken while prepping the samples for testing as they had the tendency to break upon handling.

Figure 17. The EVOH samples used in the weathering tests, with a pristine sample on the left, increasing in exposure duration from one week (right) to six weeks (left).

(a)

(b)

(c)

Figure 18. Weathered EVOH dielectric measurements plotted as ε' versus log (frequency) (a), log (ε'') versus log (frequency) (b) and a Cole-Cole representation (c).

Table 4. Low frequency fit parameters for the weathered EVOH samples where "R" stands for retest.

Sample	σ (x10^{-14} S/m)	S	$\Delta\varepsilon$	τ (s)	α	β	ε_∞
Low 2	0.06	0.63	2.05	7.67x10^{-7}	0.41	1.00	2.33
			0.38	8.02x10^{-5}	0.28	0.98	
Week 1R	1.54	1.00	0.26	8.24x10^{-4}	0.22	0.72	1.79
			1.06	1.57x10^{-7}	0.42	1.00	
Week 2	50.8	0.88	3.00	1.36x10^{-1}	0.64	1.00	1.50
			1.38	1.57x10^{-7}	0.38	1.00	
Week 2R	3.17	1.00	0.95	6.42x10^{-3}	0.09	1.00	2.29
			2.39	1.57x10^{-7}	0.42	0.94	
Week 3	11.3	1.00	0.75	7.18x10^{-1}	1.00	0.27	2.79
			3.23	1.57x10^{-7}	0.40	1.00	
Week 4	2.14	1.00	2.31	3.72x10^{7}	0.13	1.00	1.94
			1.16	1.57x10^{-7}	0.41	0.92	
Week 5	4.55	1.00	677.1	1.46x10^{7}	1.00	0.40	2.32
			2.21	1.57x10^{-7}	0.37	1.00	
Week 6	7.35	1.00	42.2	6.11x10^{4}	0.35	0.93	2.52
			2.41	1.57x10^{-7}	0.40	0.99	

4.1.2.2 FTIR Measurements

After the six weeks of weathering, FTIR measurements were performed on the six week sample to examine if any chemical changes occurred within the polymer. The only noticeable changed observed within the spectrum was the appearance of a new peak around 1709 cm^{-1} (Figure 19). This value corresponds to the oxidation of the polymer by the replacement of the hydroxyl groups with C=O bonds within the vinyl alcohol groups [24].
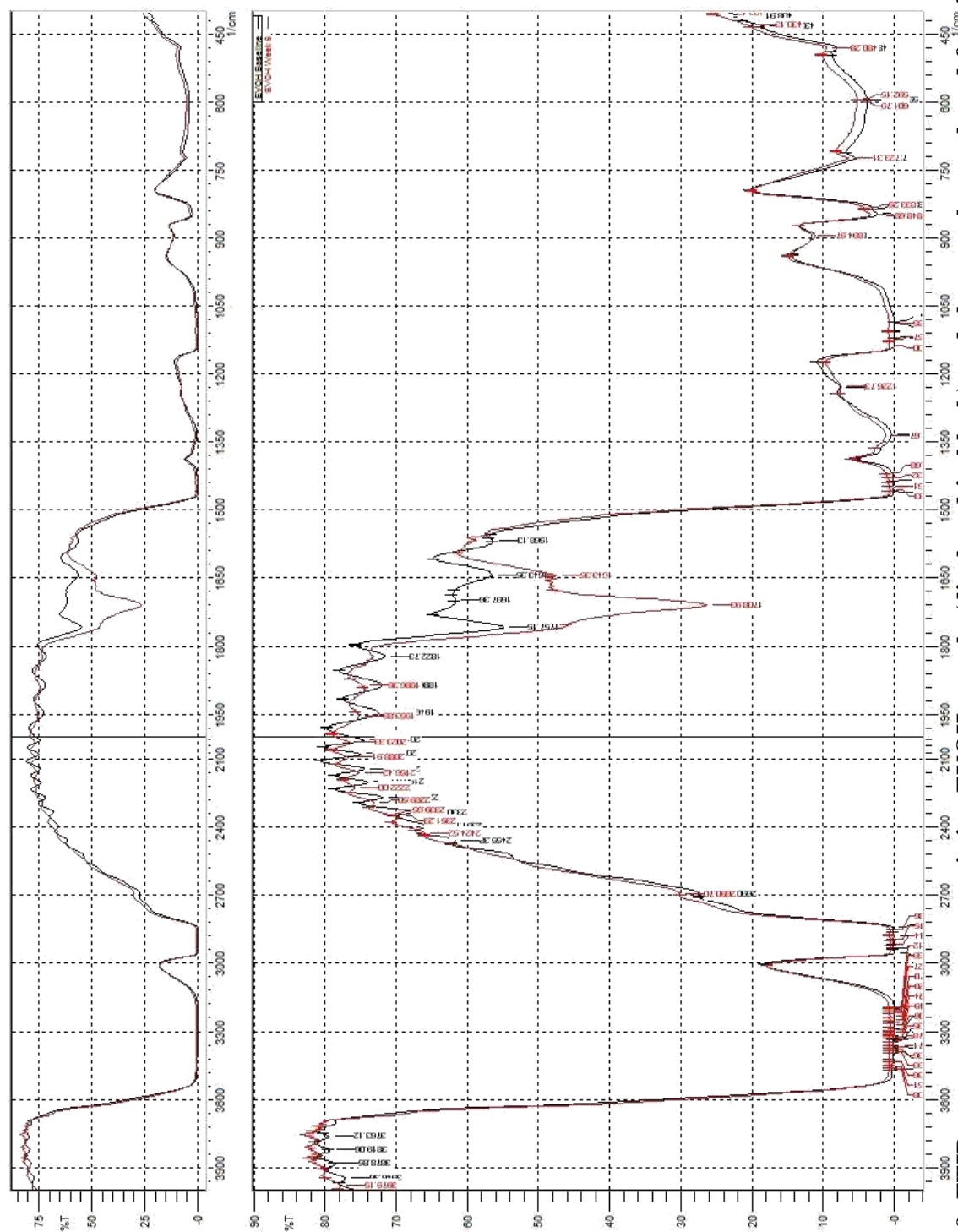
Figure 19. FTIR measurements on a pristine EVOH sample (displayed in black) and the sample weathered for six weeks (displayed in red), showing the formation of a peak around 1709 cm^{-1}.

4.1.3 Thermal Degradation Experiment

EVOH exhibited an increase in both ε' and ε'', compared to the pristine results, after thermal exposure at 100 °C began (marked by red arrows in Figure 20(a) and (b), respectively). At 1 kHz ε' increased from about 4.9 to approximately 5.9 after one week of exposure, which was greater than the pristine sample variance observed. The increase in ε'' values were more subtle but still followed the same trend as ε'. The anomalously high values of permittivity measured at 24 hours are likely due to the uncertainties associated with the measurement process discussed at the beginning of this chapter.

A shift in the relaxation frequency from about 150 kHz, for the pristine sample, to about 30 kHz after one week of thermal aging was observed (marked by a red arrow in Figure 20(b)). This is likely due to possible cross-linking and chain entanglement caused by the simultaneous thermal and ultraviolet radiation exposure. With more tightly bound chains and their functional groups, they would exhibit this lowering in relaxation frequency.

After analysis was performed on the thermally aged samples, a general increase in $\Delta\varepsilon$ was observed for both relaxations. In addition to this increase, the conductivity, MWS relaxation frequency and ε_∞ were found to increase with increased thermal aging (as shown by the fit parameters in Table 5. The exponential, α and β parameters showed no significant changes.
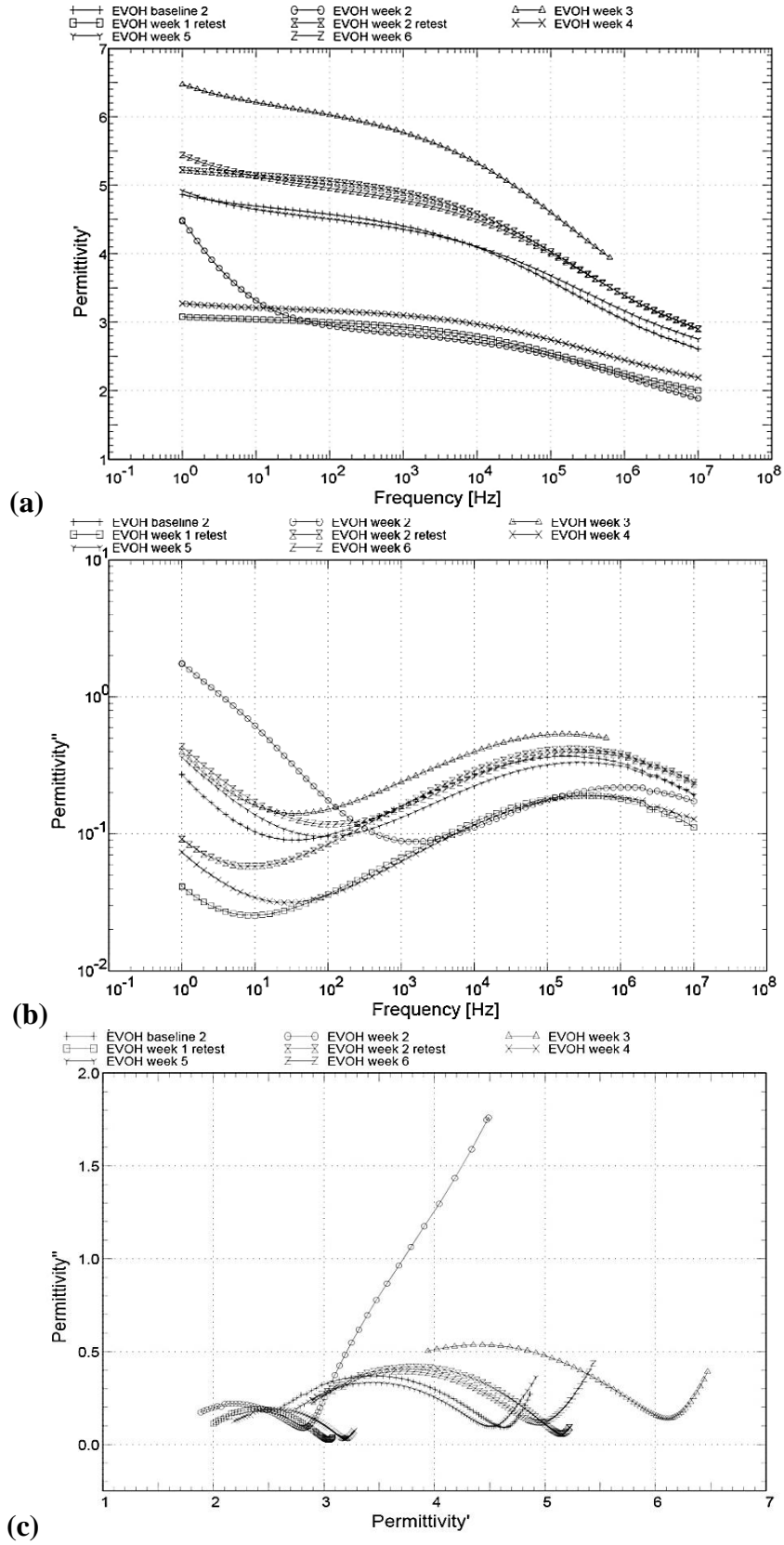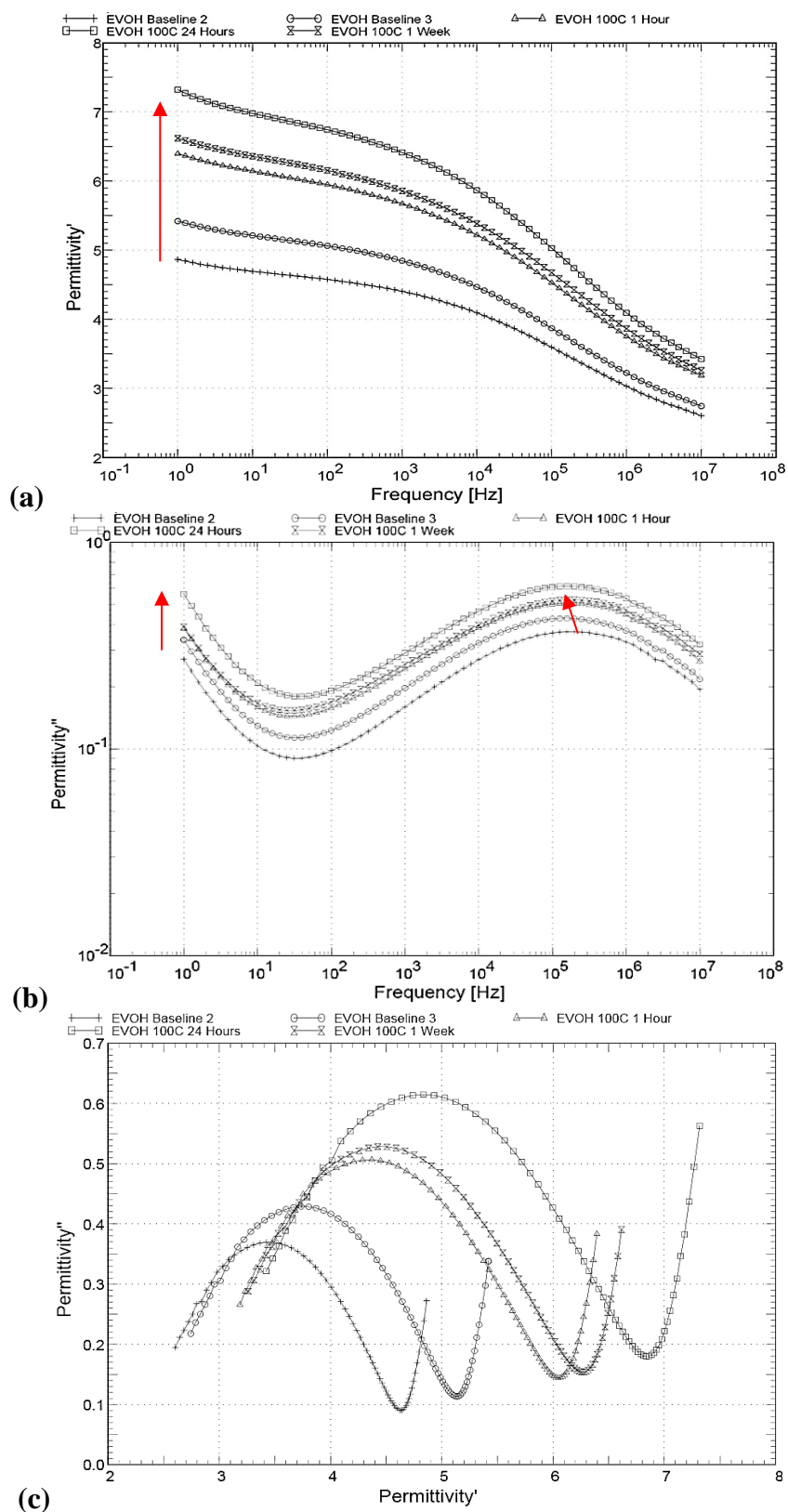
Figure 20. Thermally aged EVOH dielectric measurements plotted as ε' versus log (frequency) (a), log (ε'') versus log (frequency) (b) and a Cole-Cole representation (c). The red arrows indicate trends present within the data.

Table 5. Low frequency fit parameters for the thermally aged EVOH samples.

Sample	σ (x10^{-13} S/m)	S	$\Delta\varepsilon$	τ (s)	α	β	ε_∞
Low 2	0.60	0.63	2.05	7.67x10^{-7}	0.41	1.00	2.23
			0.38	8.02x10^{-5}	0.28	0.98	
Low 3	0.87	0.64	2.44	9.12x10^{-7}	0.40	1.00	2.34
			0.42	1.73x10^{-4}	0.28	1.00	
1 Hour	1.00	0.63	2.49	7.12x10^{-7}	0.42	1.00	2.68
			1.01	3.38x10^{-5}	0.27	1.00	
24 Hours	1.99	0.66	2.60	8.25x10^{-7}	0.43	1.00	2.76
			1.72	7.89x10^{-6}	0.24	1.00	
1 Week	1.03	0.64	2.06	6.66x10^{-7}	0.44	1.00	2.66
			1.72	7.05x10^{-6}	0.26	1.00	

4.2 Poly (Ether Ether Ketone)

4.2.1 Pristine PEEK Dielectric Measurements

A high degree of variance was observed within the dielectric measurements of the pristine PEEK samples, shown in Figure 21(a). Values of ε' at 1 kHz ranged from about 2.54 to 2.85 with an average value of 2.6 ± 0.1, which is approximately 5% variance between samples. This is likely due to the variations between samples and thickness variations across each sample as discussed at the beginning of the chapter. Also, the increase in ε' and ε'' above 2 GHz is due to a calibration error within the Novocontrol system and should not be considered part of the material response.

PEEK did exhibit one observable relaxation around 400 kHz, shown in Figure 21(b), and another small, low frequency relaxation shown by the small hump in Figure 21(c). Based on literature results, the relaxation around 400 kHz is likely the β-relaxation and the lower frequency relaxation is like due to Maxwell-Wagner-Sillars (MWS) effects [12]. A small amount of low frequency conductivity was measured within the samples, which increased slightly as the frequency decreased below 1 Hz. An example fit of the β-relaxation, MWS

effects and conductivity obtained by the HN model for sample "Low 1" is plotted in Figure

22 with the corresponding fit parameters shown in Table 6.
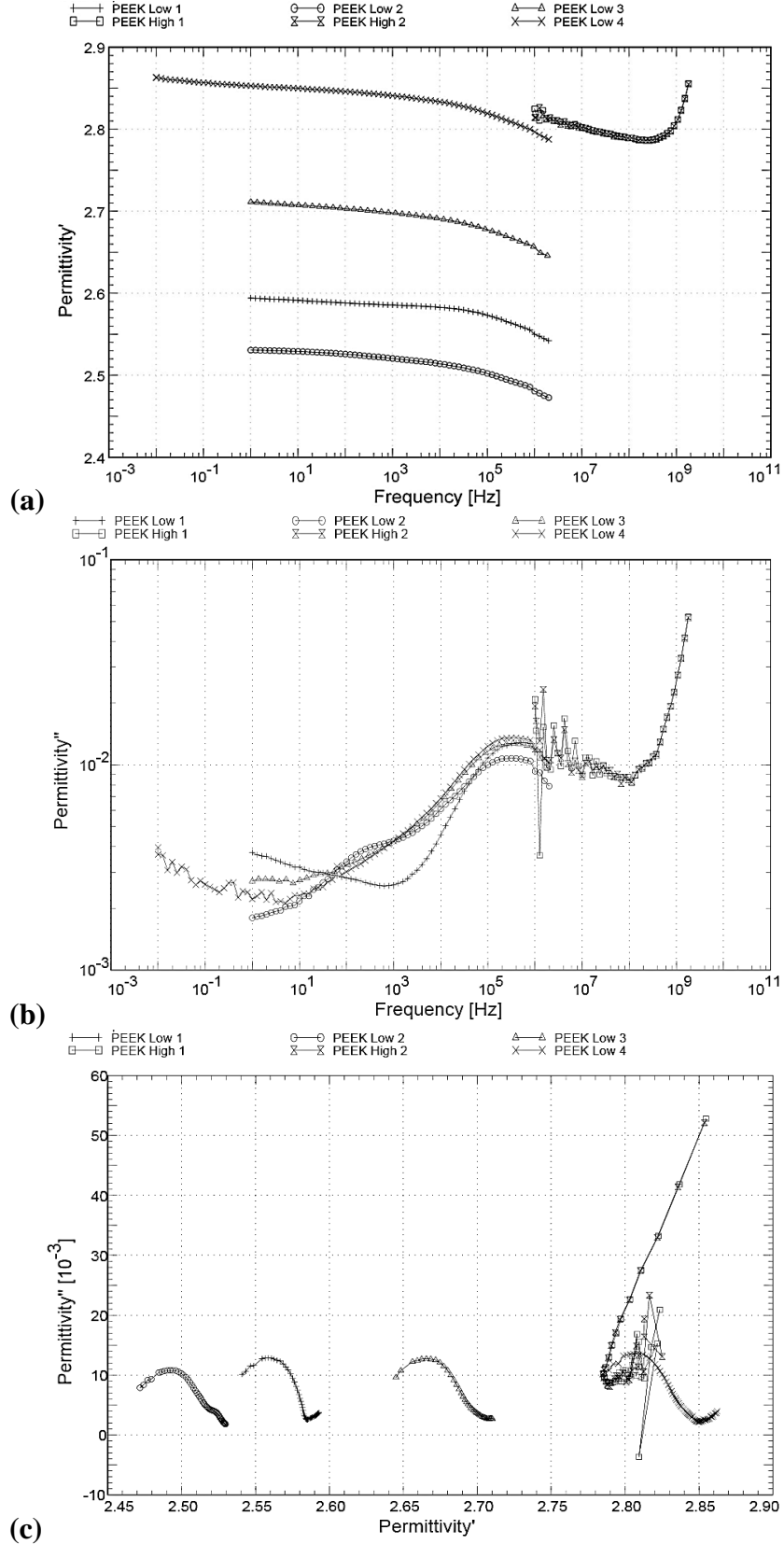
Figure 21. Pristine PEEK dielectric measurements plotted as ε' versus log (frequency) (a), log (ε'') versus log (frequency) (b) and a Cole-Cole representation (c).
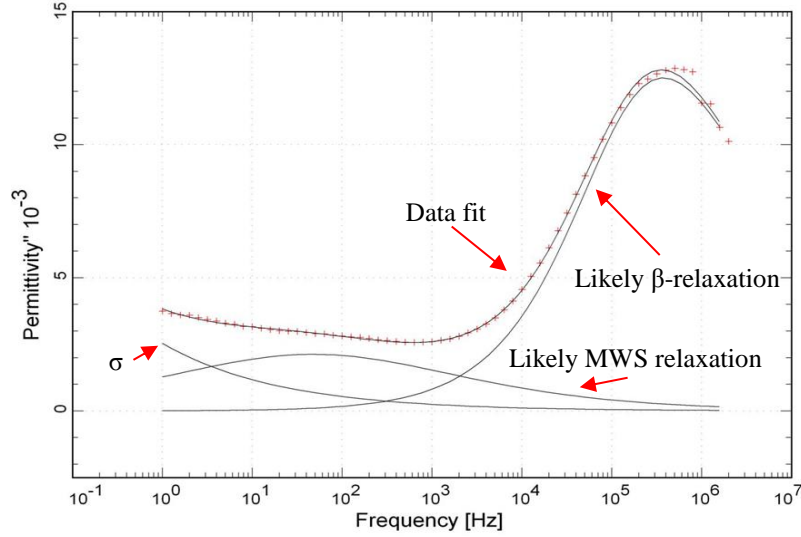
Figure 22. The data fit produced by the Havriliak-Negami function in WinFit on the pristine PEEK sample Low 1 plotted as ε'' verses log (frequency).

Table 6. Low frequency fit parameters for pristine PEEK.

Sample	σ (x10^{-20} S/m)	S	$\Delta\varepsilon$ (x10^{-2})	τ (s)	α	β	ε_∞
Low 1	1.00	0.34	5.80	1.13×10^{-6}	0.68	0.48	2.43
			1.42	3.34×10^{-3}	0.43	1.00	
Low 2	1.00	0.38	4.52	7.06×10^{-7}	0.58	0.82	2.37
			1.79	3.65×10^{-4}	0.43	1.00	
Low 3	1.00	0.38	4.19	4.57×10^{-7}	0.59	1.00	2.54
			3.74	5.25×10^{-5}	0.21	1.00	
Low 4	1.00	0.45	4.19	5.32×10^{-7}	0.56	1.00	2.62
			10.49	1.62×10^{-9}	0.09	0.98	

4.2.2 Weathering Experiment

4.2.2.1 Dielectric Measurements

With increasing exposure, in general, both ε' and ε'' increased with time (indicated by red arrows in Figure 24(a) and (b) respectively). The ε' values fall within the original range of the pristine PEEK samples; however, only weeks one and three are within one standard deviation of the mean pristine values and the other weeks tested are above this range. A comparison of the physical changes can be seen in Figure 23. A small increase in

conductivity was observed with increasing time but a large increase, comparatively, was seen after week six, Figure 24(b) and (c). Also, the β-relaxation frequency decreased with increasing exposure time, from about 300 kHz to 100 kHz after week six.

During the exposure period, no clear trends were observed within the fit parameters (Table 7) except for a general increase in $\Delta\varepsilon$ of the MWS relaxation and ε_∞ increased each week. The large amount of conductivity present in the Week 2 sample is likely due to excess water left over from the weathering cycle that was still present during the dielectric measurements.
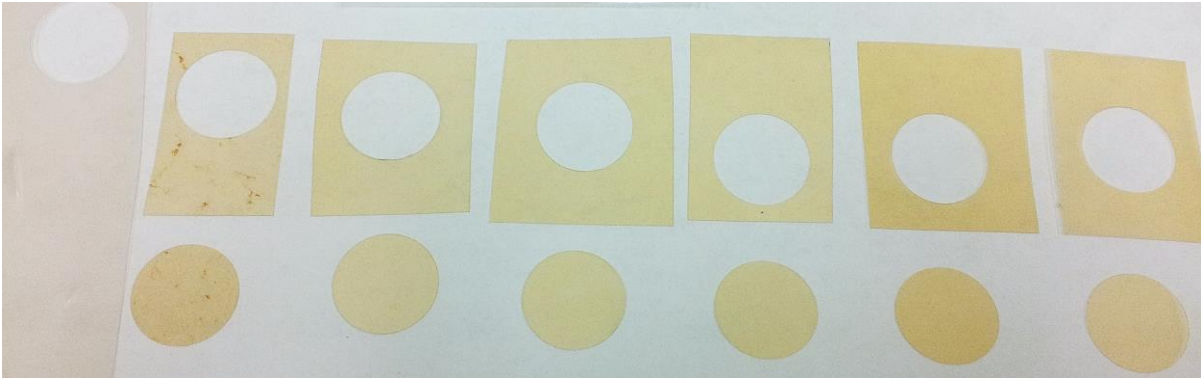
Figure 23. The PEEK samples used in the weathering tests, with a pristine sample on the left, increasing in exposure duration from one week to six weeks while moving to the right.
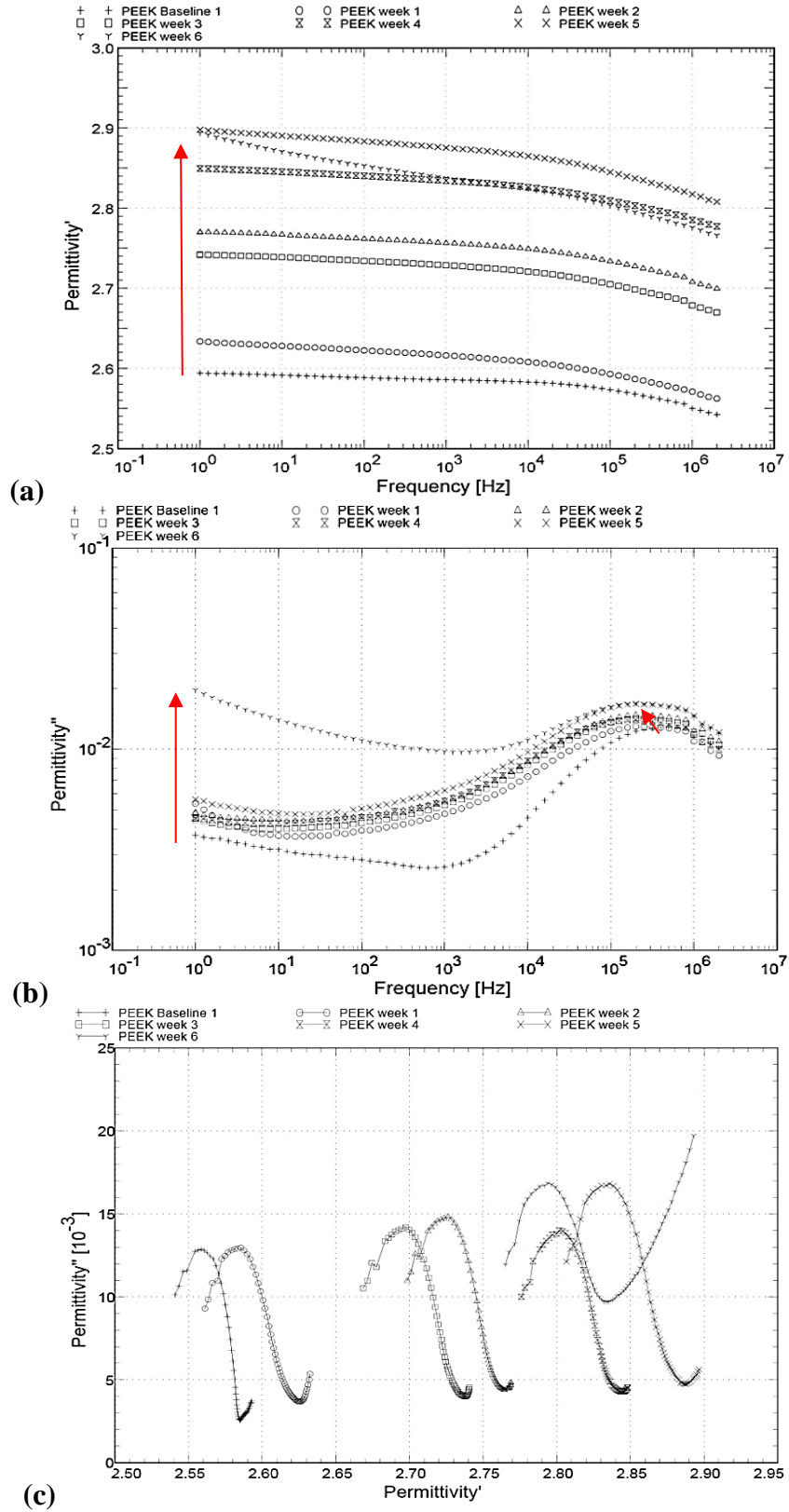
Figure 24. Weathered PEEK dielectric measurements plotted as ε' versus log (frequency) (a), log (ε'') versus log (frequency) (b) and a Cole-Cole representation (c). The red arrows indicate trends present within the data.

Table 7. Low frequency fit parameters for the weathered PEEK samples.

Sample	σ (x10^{-20} S/m)	S	$\Delta\varepsilon$ (x10^{-2})	τ (s)	α	β	ε_∞
Low 1	1.00	0.35	5.80	1.13x10^{-6}	0.68	0.48	2.52
			1.42	3.34x10^{-3}	0.37	1.00	
Week 1	3517	0.59	5.06	5.44x10^{-7}	0.56	1.00	2.55
			2.87	7.06x10^{-4}	0.29	1.00	
Week 2	1.00	0.33	4.59	6.56x10^{-7}	0.58	1.00	2.56
			1.66	1.30x10^{-1}	0.40	0.05	
Week 3	1.02	0.33	5.31	8.92x10^{-7}	0.57	0.81	2.65
			4.26	1.20x10^{-2}	0.37	0.26	
Week 4	1.00	0.34	5.39	1.08x10^{-6}	0.56	0.80	2.76
			4.40	2.66x10^{-2}	0.35	0.29	
Week 5	1.01	0.31	5.57	7.48x10^{-7}	0.60	0.88	2.79
			5.48	1.53x10^{-3}	0.28	0.41	
Week 6	370.5	0.38	5.80	7.12x10^{-7}	0.59	0.87	2.75
			10.20	1.10x10^{-2}	0.24	1.00	

4.2.2.2 FTIR Measurements

When compared to the pristine FTIR measurements (Figure 25), the sample weathered for six weeks exhibited a decrease in transmission between 3650 and 3150 cm^{-1}. These wavenumbers correspond to the presence of alcohol groups (~3600-3200 cm^{-1}), likely present due to the formation of free radicals. Free radicals are formed when the ultraviolet radiation interacts with the hydrogen bonds and create a free ion, allowing for its interaction with other polymer chains and any chemical species present in the polymer (typically oxygen or hydroxyls). As the number of free radicals increases, the amount of damage also increases. A second depression in the measured IR transmission on samples weathered for six weeks occurs around 1772 cm^{-1}. This wavenumber corresponds to the stretching of the carbonyl groups (C=O) within the polymer chains [18, 24].
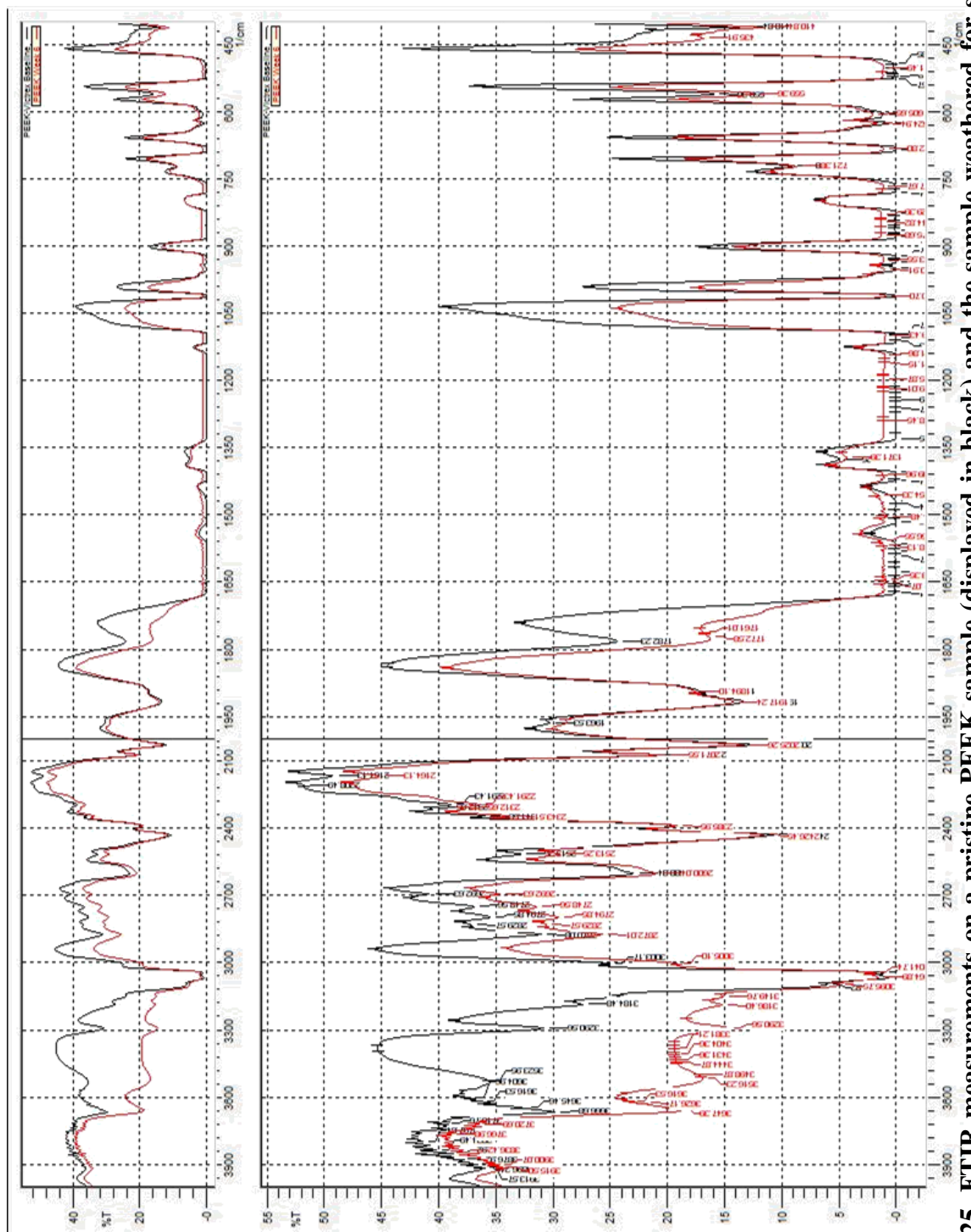
Figure 25. FTIR measurements on a pristine PEEK sample (displayed in black) and the sample weathered for six weeks (displayed in red), showing a decrease in peak intensity from 3650 to 3150 cm⁻¹.

4.2.3 Thermal Degradation Experiment

In general, as the thermal aging progressed at 300 °C, ε' increased (shown in Figure 27(a)) and at 1 kHz all the aged samples had ε' values greater than that of the pristine sample. The ε'' values (shown in Figure 27(b)) suggest a decrease in the relaxation frequency from about 250 kHz to 200 kHz after one week, indicated by a red arrow in Figure 27(b) and the fit parameters in Table 8, and an increase in ε_∞. This slight decrease in relaxation frequency is likely attributed to some degree of chain entanglement restricting movement of the aromatic rings. A slight shrinking and darkening of the material was observed with increasing exposure (Figure 26).

Figure 26. The PEEK samples used for thermal aging, with a pristine sample on the left, increasing in exposure duration at 300°C from one hour, to 24 hours, to one week while moving to the right.
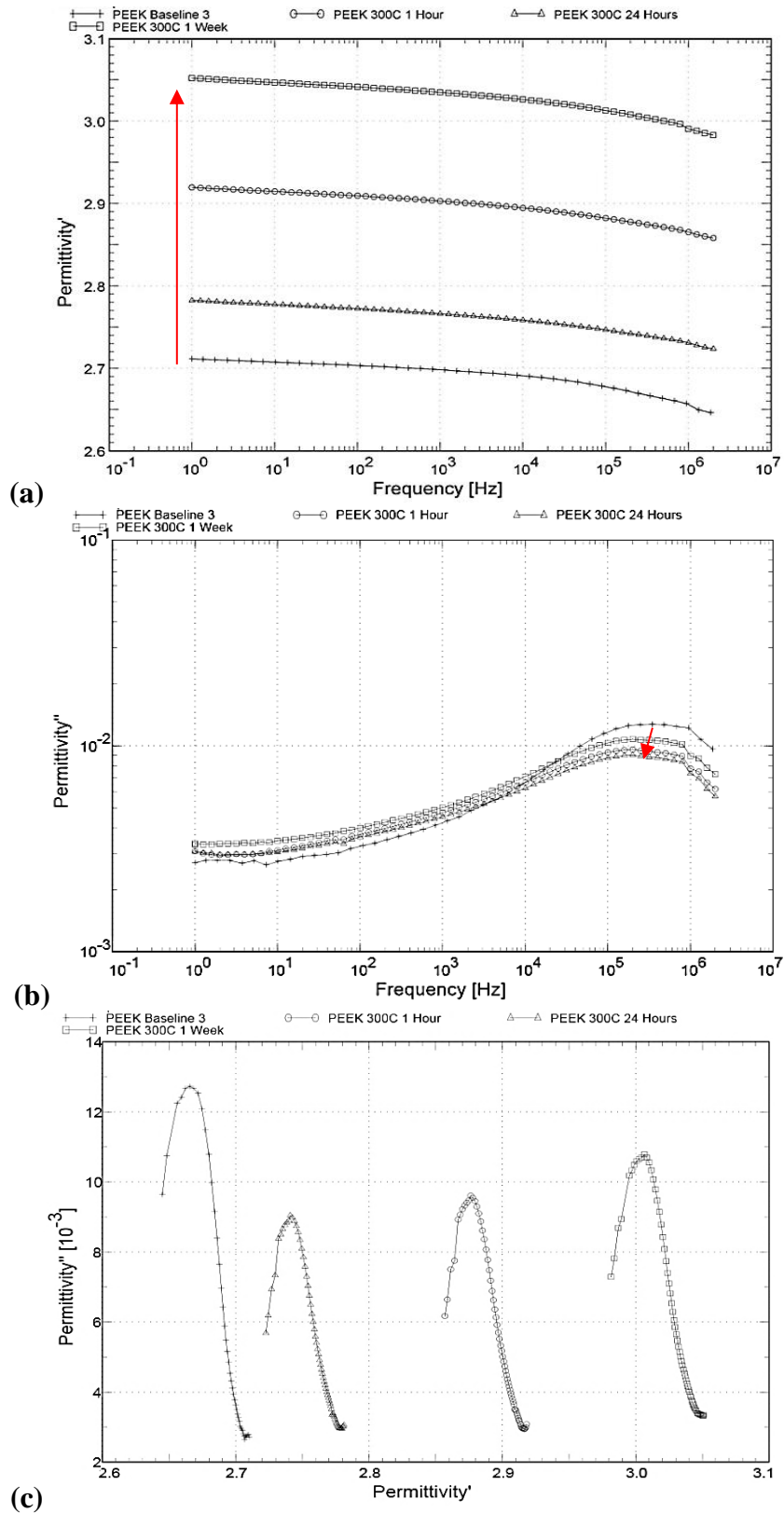
Figure 27. Thermally aged PEEK dielectric measurements plotted as ε' versus log (frequency) (a), log (ε'') versus log (frequency) (b) and a Cole-Cole representation (c). The red arrows indicate trends present within the data.

Table 8. Low frequency fit parameters for the thermally aged PEEK samples.

Sample	σ (x10^{-20} S/m)	S	$\Delta\varepsilon$ (x10^{-2})	τ (s)	α	β	ε_∞
Low 2	1.00	0.38	4.52	7.06x10^{-7}	0.58	0.82	2.37
			1.79	3.65x10^{-4}	0.43	1.00	
Low 3	1.00	0.38	4.19	4.57x10^{-7}	0.59	1.00	2.54
			3.74	5.25x10^{-5}	0.21	1.00	
1 Hour	1.00	0.36	2.97	6.17x10^{-7}	0.57	1.00	2.76
			3.42	8.48x10^{-5}	0.28	1.00	
24 Hours	1.00	0.36	2.68	6.16x10^{-7}	0.59	1.00	2.62
			3.32	7.75x10^{-5}	0.28	1.00	
1 Week	1.00	0.36	3.43	5.73x10^{-7}	0.57	1.00	2.88
			3.88	1.02x10^{-4}	0.25	1.00	

4.3 Polyphenylene Sulfide

4.3.1 Pristine PPS Dielectric Measurements

A 4 % variance was observed within the dielectric measurements of the pristine PPS samples while almost no variation was observed in ε''. Values of ε' at 1 kHz ranged from about 2.55 to 2.83, shown in Figure 28(a), with a mean value of 2.6 ± 0.1. The increase in ε' and ε'' above 2 GHz is due to a calibration error within the Novocontrol system and should not be considered part of the material response.

A possible relaxation was observed above 1 MHz, shown in Figure 28(b). Based on literature results, this relaxation is likely the β_I-relaxation [15]. The β_{II}-relaxation is typically observed at higher frequency [15] and has almost no effect within the frequency range examined at room temperature. A small amount of low frequency conductivity was measured below 1 Hz within the samples. An example fit of the β-relaxations and conductivity obtained by the HN model for sample "Low 1" is plotted in Figure 29 with the corresponding fit parameters shown in Table 9.
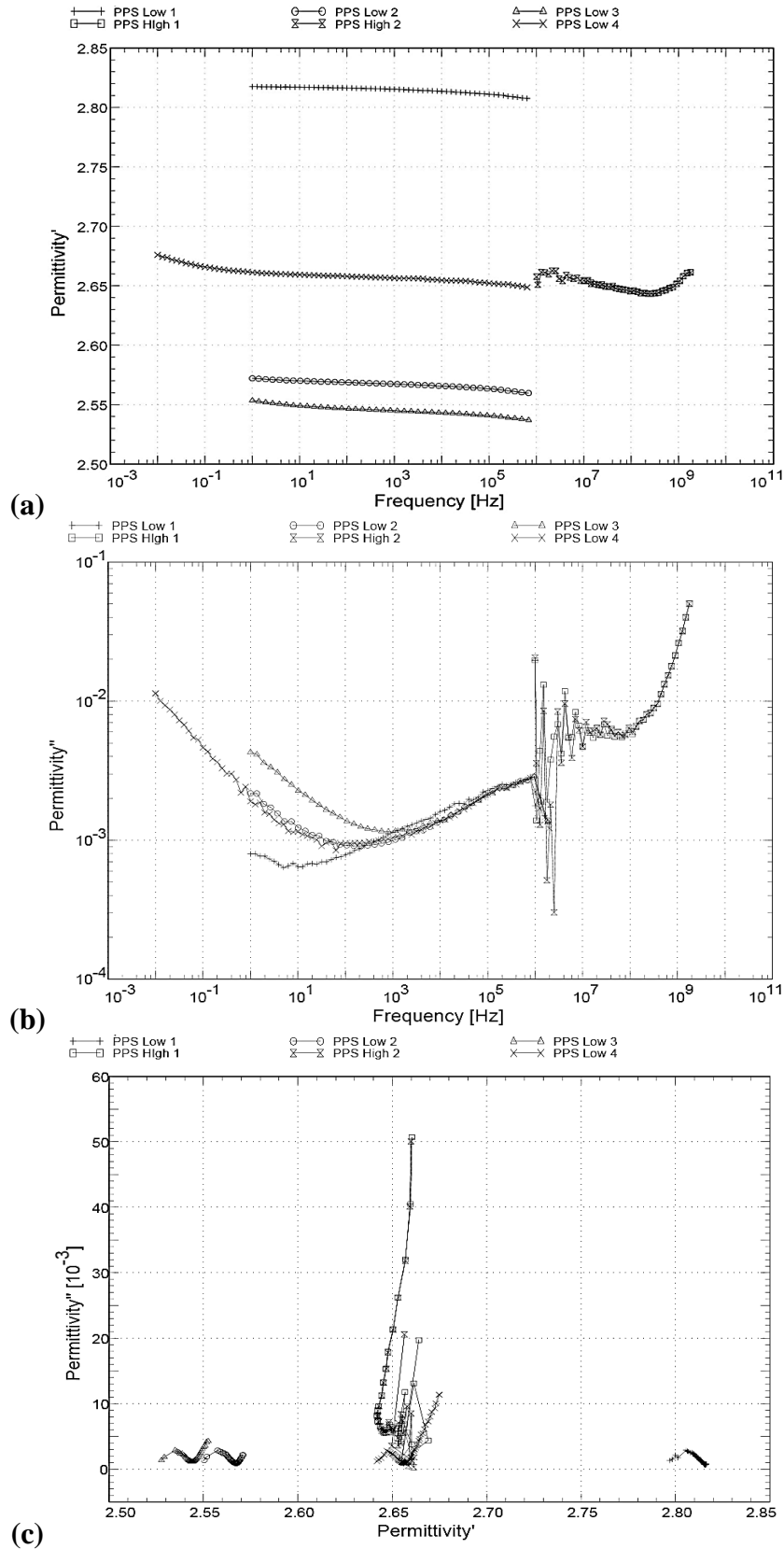
Figure 28. Pristine PPS dielectric measurements plotted as *ε'* versus log (frequency) (a), log (*ε''*) versus log (frequency) (b) and a Cole-Cole representation (c).
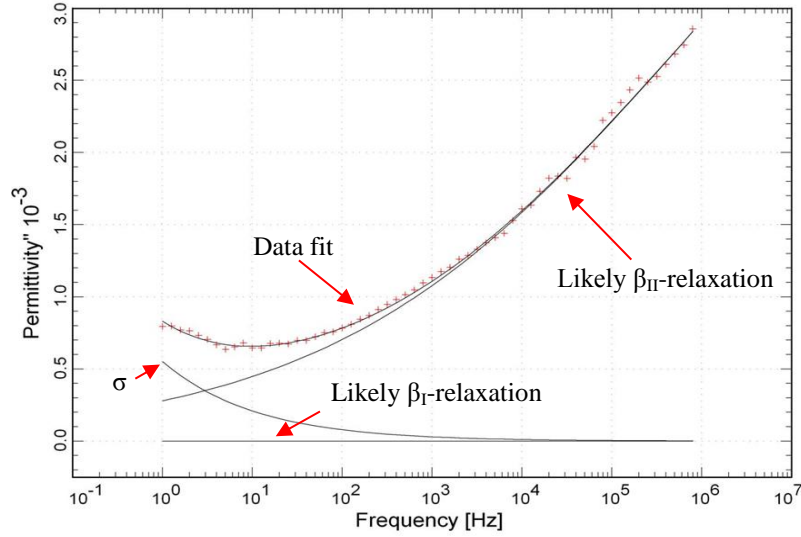
Figure 29. The data fit produced by the Havriliak-Negami function in WinFit on the pristine PPS sample Low 1 plotted as ε'' verses log (frequency).

Table 9. Low frequency fit parameters for pristine PPS.

Sample	σ (x10^{-20} S/m)	S	$\Delta\varepsilon$	τ (s)	α	β	ε_∞
Low 1	1.06	0.42	4.65×10^{-1}	1.93×10^{-7}	0.22	0.04	2.73
			1.00×10^{-6}	1.00×10^{-11}	0.01	0.40	
Low 2	1.00	0.35	4.13×10^{-1}	2.61×10^{-7}	0.29	0.03	2.34
			10.23×10^{-1}	1.00×10^{-11}	0.01	0.01	
Low 3	1.00	0.31	3.42×10^{-1}	7.39×10^{-7}	0.34	0.02	2.24
			1.13×10^{-1}	1.00×10^{-11}	0.01	0.03	
Low 4	5.83	0.39	22.17×10^{-1}	9.21×10^{-10}	0.21	0.02	2.44
			1.10×10^{-4}	9.10×10^{-4}	1.00	1.00	

4.3.2 Weathering Experiment

4.3.2.1 Dielectric Measurements

With increasing exposure, ε', ε'' and the amount of conductivity increased with time (marked by red arrows in Figure 31(a) and (b) respectively). The large increase in low frequency conductivity (shown in Table 10) masks the physical effects going on within this range but it appears that the β_{II}-relaxation shifted from 1+ MHz to roughly 600 kHz and a second relaxation appeared after three weeks around 300 Hz and shifted to roughly 2 Hz after

six weeks (marked by red arrows in Figure 31(b). These changes are likely due to the heavy thermal/radiation damage seen by the darkening of the samples in Figure 30 after one week. Each of the increases observed in ε' were greater than the mean pristine sample variance observed but the initial increases were within the variance associated with the pristine baseline measurement.
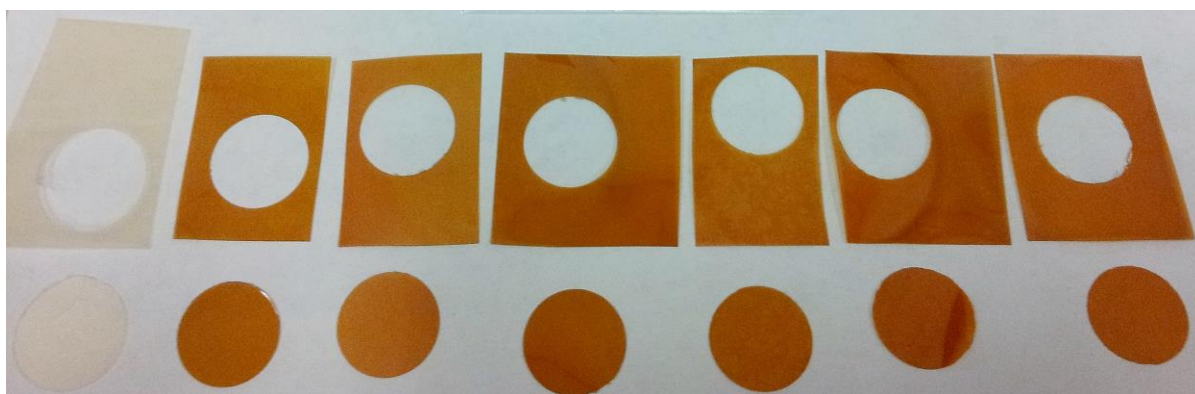
Figure 30. The PPS samples used in the weathering tests, with a pristine sample on the left, increasing in exposure duration from one week to six weeks while moving to the right.
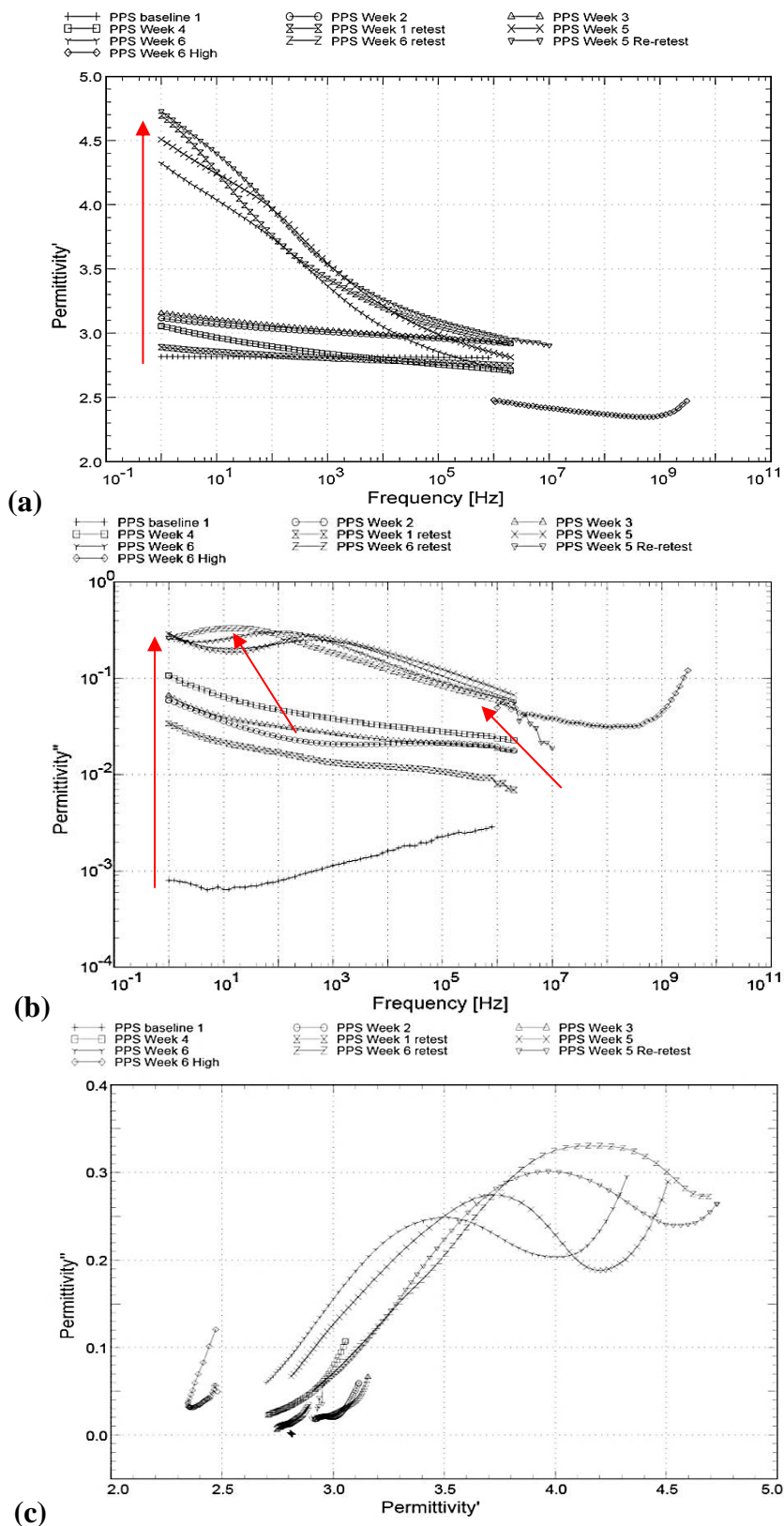
Figure 31. Weathered PPS dielectric measurements plotted as *ε'* versus log (frequency) (a), log (*ε''*) versus log (frequency) (b) and a Cole-Cole representation (c). The red arrows indicate trends present within the data.

Table 10. Low frequency fit parameters for the weathered PPS samples where "R" stands for retest.

Sample	σ (S/m)	S	$\Delta\varepsilon$	τ (s)	α	β	ε_∞
Low 1	1.06×10^{-20}	0.42	4.65×10^{-1}	1.93×10^{-7}	0.22	0.04	2.35
			1.00×10^{-6}	1.00×10^{-11}	0.01	0.40	
Week 1R	9.34×10^{-17}	0.41	6.65×10^{-2}	1.12×10^{-2}	0.48	0.58	2.74
			5.78×10^{-2}	1.75×10^{-6}	0.36	1.00	
Week 2	3.21×10^{-18}	0.24	1.32×10^{-1}	8.83×10^{-4}	0.59	0.04	2.81
			9.93×10^{-2}	5.97×10^{-7}	0.35	1.00	
Week 3	1.09×10^{-15}	0.47	3.07×10^{-1}	3.60×10^{-2}	0.45	0.20	2.82
			2.09×10^{-2}	2.61×10^{-7}	0.53	1.00	
Week 4	3.43×10^{-16}	0.32	3.09×10^{-1}	6.75×10^{-3}	0.40	0.24	2.62
			4.13×10^{-2}	1.90×10^{-7}	0.39	1.00	
Week 5	2.72×10^{-14}	0.53	4.25×10^{-1}	9.76×10^{-4}	0.95	0.36	2.67
			1.52	3.29×10^{-4}	0.25	1.00	
Week 5R	3.19×10^{-14}	0.91	7.50×10^{-1}	1.24×10^{-3}	0.55	1.00	2.54
			3.42	$3.61\times10^{+1}$	0.13	0.78	
Week 6	9.02×10^{-15}	0.34	1.13	8.37×10^{-4}	0.57	0.47	2.39
			7.83×10^{-1}	$7.45\times10^{+3}$	1.00	0.04	
Week 6R	3.25×10^{-14}	0.97	1.61	1.07×10^{-2}	0.48	1.00	2.66
			6.96×10^{-1}	2.27×10^{-4}	0.64	0.18	

4.3.2.2 FTIR Measurements

Many possible changes were observed in the FTIR transmission spectra when comparing pristine samples and those weathered for six weeks. Changes were observed for wavenumbers (from left to right in Figure 32) 3300-3100, 1716, 1321, 1273-1200, 1150, 1050, 900, and 623 cm^{-1}. The highest wavenumbers correspond to the presence of hydroxyl groups within the polymer and 1716 cm^{-1} shows the presence of carbonyl groups. Also, the wavenumbers 1321, 1273-1200, 1150, and 1050 cm^{-1} are all associated with the stretching of C-O bonds within the aromatic ring. The absorption at 900 cm^{-1} suggests the possibility of either =C-O bonding or a meta substituted aromatic ring. This ring structure occurs when the sulfur of a repeating unit cell bonds to a neighboring carbon. The peak around 900 cm^{-1} is possibly due to the presence of alkyne groups. All of these show that extensive bonding and chemical changes have occurred due to heavy oxidation.
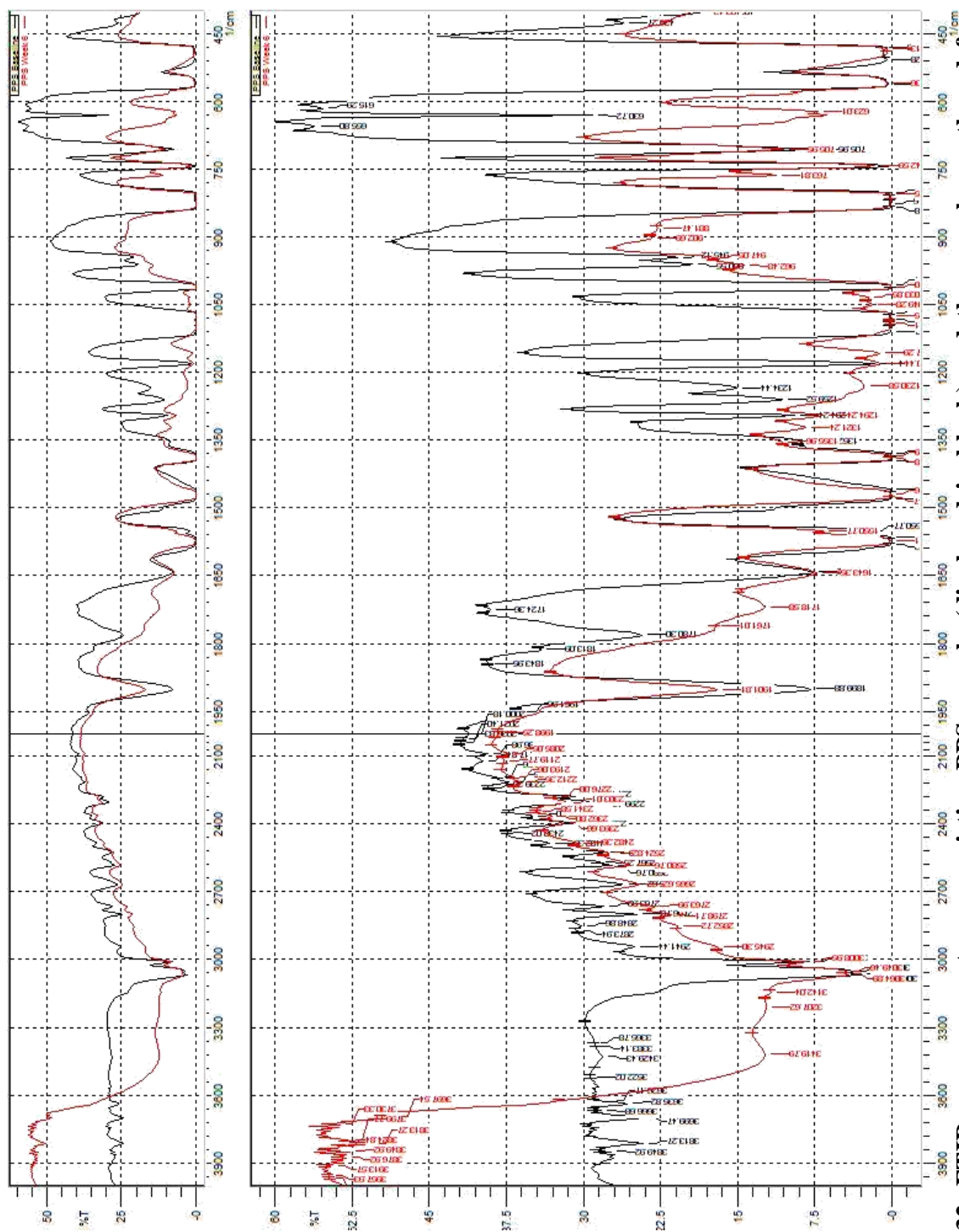
Figure 32. FTIR measurements on a pristine PPS sample (displayed in black) and the sample weathered for six weeks (displayed in red), showing possible changes around 3300-3100, 1716, 1321, 1273-1200, 1150, 1050, 900, and 623 cm⁻¹ .

4.3.3 Thermal Degradation Experiment

After one week of thermal exposure at 200 °C the β_{II}-relaxation shifted from 1+ MHz to roughly 200 kHz but no other significant results were observed. The spurious data above 250 kHz are due to sources of the uncertainties and errors discussed at the beginning of the chapter. Real permittivities values obtained during the week of thermal aging were within one standard deviation of the mean value measured on pristine and can be considered as representing no significant change. During thermal aging, a slight decrease in $\Delta\varepsilon$ of the β_{II}-relaxation (shown in Table 11) and a stiffening/shrinking of the samples was observed (Figure 33). No other noteworthy changes were observed.
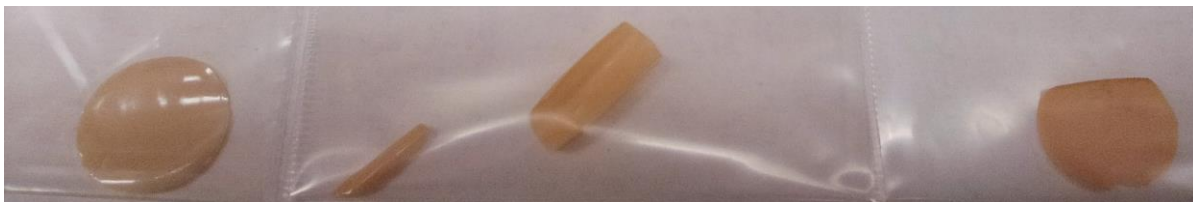
Figure 33. The PPS samples used for thermal aging, with a pristine sample on the left, increasing in exposure duration at 300°C from one hour, to 24 hours, to one week while moving to the right.
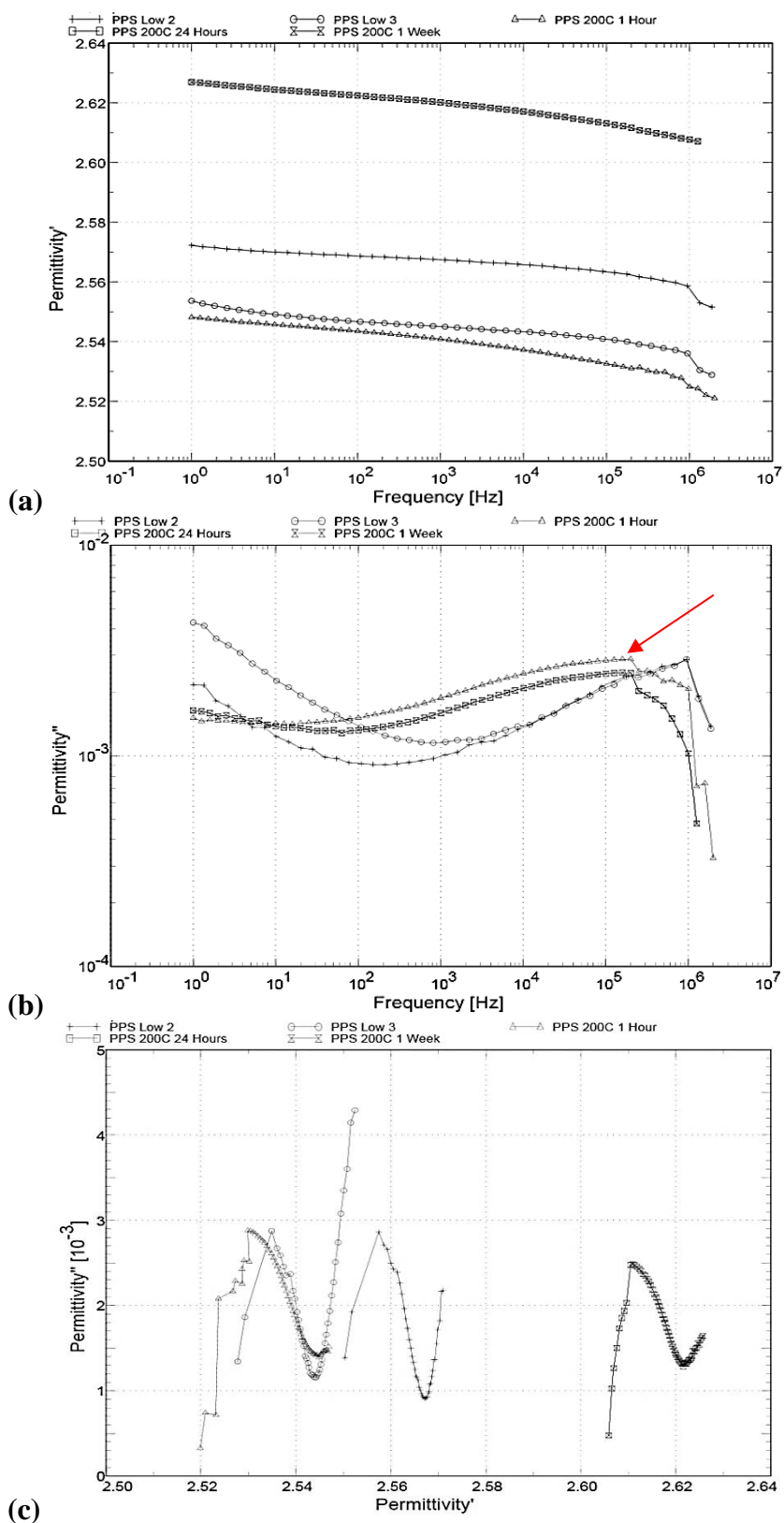
Figure 34. Thermally aged PPS dielectric measurements plotted as ε' versus log (frequency) (a), log (ε'') versus log (frequency) (b) and a Cole-Cole representation (c). The red arrow indicates trends present within the data.

Table 11. Low frequency fit parameters for the thermally aged PPS samples.

Sample	σ (x10^{-20} S/m)	S	$\Delta\varepsilon$	τ (s)	α	β	ε_∞
Low 2	1.00	0.35	0.39	3.24x10^{-7}	0.30	0.03	2.34
			1.36	1.00x10^{-11}	0.01	0.01	
Low 3	1.00	0.31	0.20	5.51x10^{-7}	0.33	0.05	2.24
			0.11	6.06x10^{-7}	0.12	0.01	
1 Hour	1.00	0.46	0.17	4.61x10^{-11}	0.59	0.01	2.00
			0.41	2.54x10^{-5}	0.03	0.17	
24 Hours	1.00	0.41	0.11	3.81x10^{-7}	0.66	0.01	2.15
			0.39	2.12x10^{-5}	0.03	0.17	
1 Week	1.00	0.41	0.11	3.81x10^{-5}	0.63	0.01	2.17
			0.38	3.87x10^{-10}	0.03	0.19	

4.4 Ultra-High Molecular Weight Polyethylene

4.4.1 Pristine UHMWPE Dielectric Measurements

UHMWPE shows relatively consistent and featureless ε' and ε'' spectra within this frequency range, Figure 35(a) and (b) respectively. At low frequency the ε' values have a low variance (about 1%) and a mean value of 2.07 ± 0.02, with almost zero loss. The high frequency measurements show more variability in ε', with values between 1.99 and 2.32, due to the experimental challenges with higher frequency measurements discussed at the beginning of the chapter. For the same reasons, the data above 700 MHz should be considered to be roughly the same as the data obtained between 2 MHz and 700 MHz.

Due to the low loss ($\sim 10^{-4}$), a fit of the pristine results was problematic because of the variability in the final fit parameters obtained. An example fit is shown in Figure 36 with the corresponding fit parameters for the low frequency pristine samples shown in Table 12.
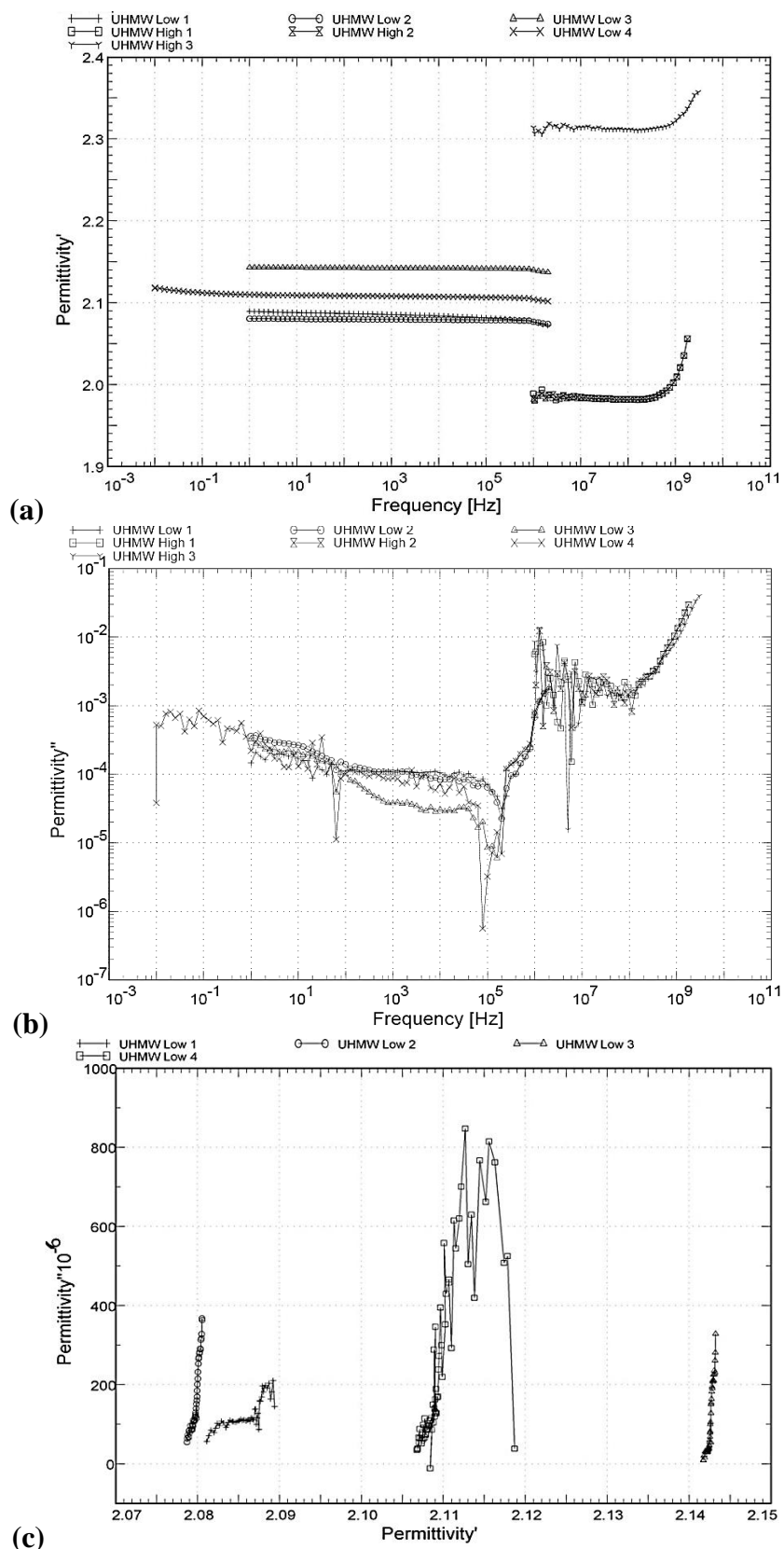
Figure 35. Pristine UHMWPE dielectric measurements plotted as ε' versus log (frequency) (a), log (ε'') versus log (frequency) (b) and a Cole-Cole representation (c).
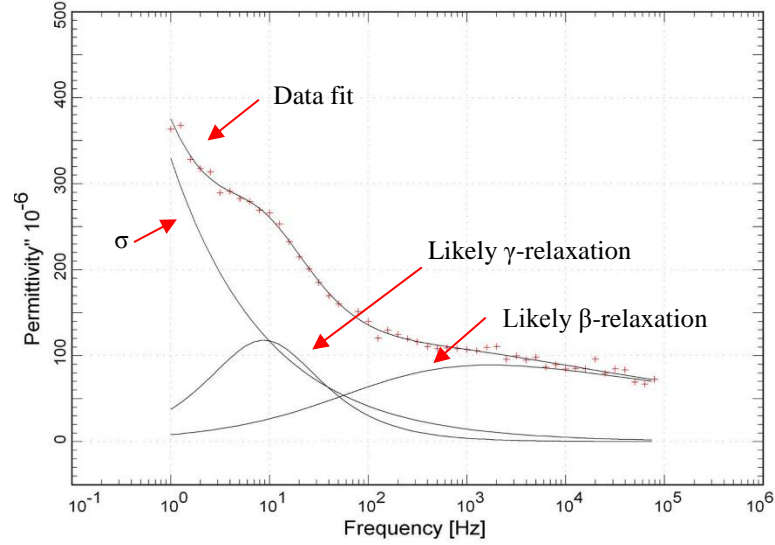
Figure 36. The data fit produced by the Havriliak-Negami function in WinFit on the pristine UHMWPE sample Low 2 plotted as ε'' verses log (frequency).

Table 12. Low frequency fit parameters for pristine UHMWPE.

Sample	σ (S/m)	S	$\Delta\varepsilon$ (x10^{-4})	τ (s)	α	β	ε_∞
Low 1	1.00×10^{-20}	0.52	2.18	3.87×10^{-2}	1.00	1.00	2.05
			13.33	4.91×10^{-3}	0.45	0.19	
Low 2	1.00×10^{-20}	0.45	2.69	1.79×10^{-2}	0.93	1.00	2.03
			8.12	1.21×10^{-3}	0.60	0.20	
Low 3	1.38×10^{-16}	1.00	5.91	2.17×10^{-2}	0.77	0.76	2.07
			1.58	7.62×10^{-5}	0.90	0.17	
Low 4	1.25×10^{-19}	0.53	2.50	7.64×10^{-3}	1.00	0.76	2.06
			3.36	2.86×10^{-4}	0.95	0.28	

4.4.2 Weathering Experiment

4.4.2.1 Dielectric Measurements

Over the six weeks of weathering the ε' values fluctuated between weeks but no significant trend was observed, Figure 38(a). The ε'' values however, were observed to increase each week, Figure 38(b), with week's 4-6 falling within one standard deviation of the mean value. This increase can be attributed to the appearance of a relaxation around 3 Hz after the second week, which shifted to lower frequencies with increasing exposure time, and

a possible relaxation around 200 kHz. The relaxation around 3 Hz is due to the γ-relaxation, which is likely caused the motion of chain fragments or defects [17]. Care had to be taken to ensure not to damage the samples during dielectric measurements as the material became brittle and started to break in the sample holder during the third week of the weathering cycle, as shown in Figure 37.

The conductivity and $\Delta\varepsilon$ values were found to, in general, increase each week (Table 13). These increases can also be explained by the presence of water (in the form of hydroxyl ions). Also, during the initial two weeks ε_∞ exhibited a slight increase but after this time, the values tended to decreased.
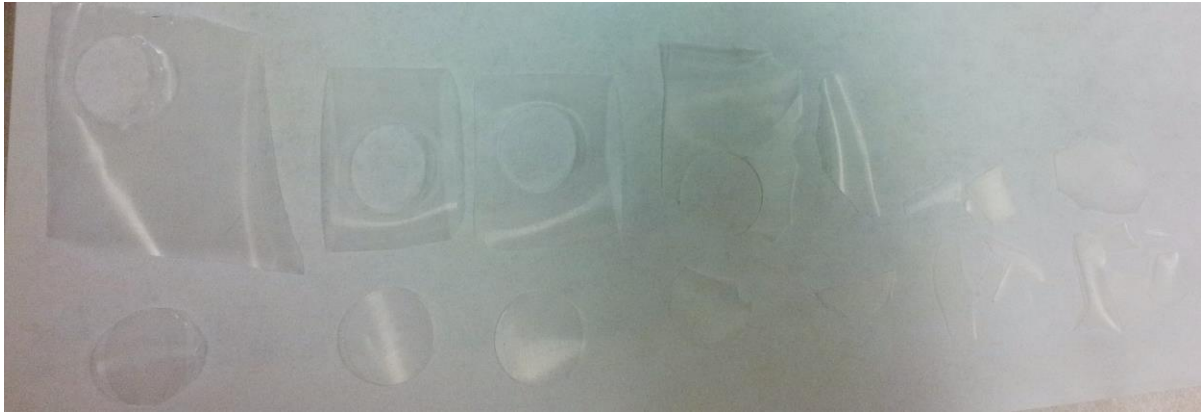
Figure 37. The UHMWPE samples used in the weathering tests, with a pristine sample on the left, increasing in exposure duration from one week to six weeks while moving to the right.
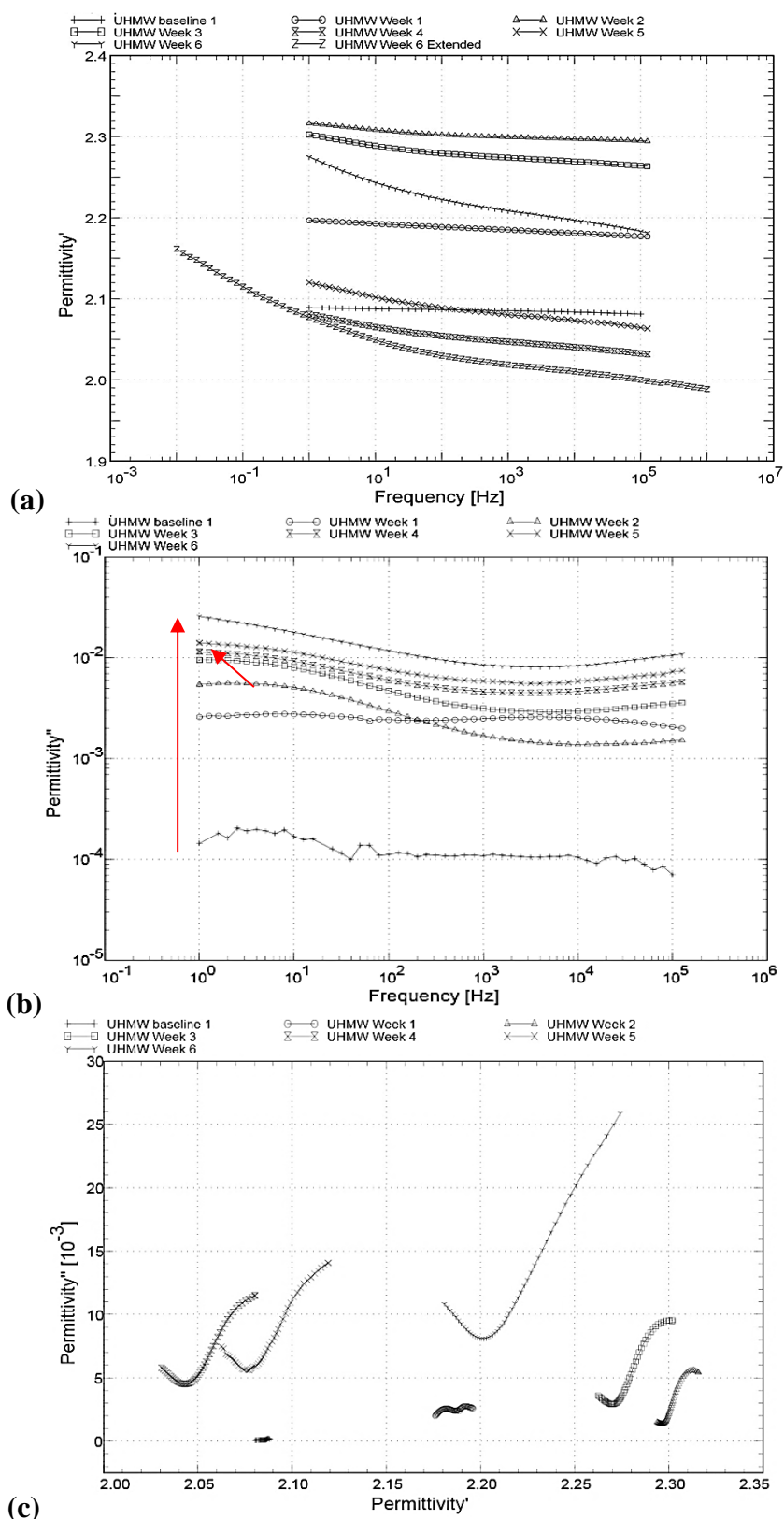
Figure 38. Weathered UHMWPE dielectric measurements plotted as *ε'* versus log (frequency) (a), log (*ε''*) versus log (frequency) (b) and a Cole-Cole representation (c). The red arrows indicate trends present within the data.

Table 13. Low frequency fit parameters for the weathered UHMWPE samples.

Sample	σ (S/m)	S	$\Delta\varepsilon$	τ (s)	α	β	ε_∞
Low 1	1.00×10^{-20}	1.00	1.71×10^{-4}	4.39×10^{-2}	1.00	1.00	2.08
			3.03×10^{-3}	$3.46 \times 10^{+1}$	0.26	0.14	
Week 1	1.02×10^{-20}	0.37	6.13×10^{-3}	2.05×10^{-2}	0.60	0.99	2.17
			1.89×10^{-2}	9.18×10^{-5}	0.40	0.55	
Week 2	1.10×10^{-20}	0.36	4.27×10^{-2}	6.75×10^{-11}	0.15	0.94	2.26
			1.85×10^{-2}	3.63×10^{-2}	0.54	1.00	
Week 3	2.56×10^{-19}	0.42	1.30×10^{-1}	1.00×10^{-11}	0.15	0.88	2.15
			3.25×10^{-2}	6.02×10^{-2}	0.51	1.00	
Week 4	3.28×10^{-17}	0.55	2.05×10^{-1}	1.00×10^{-11}	0.17	0.94	1.85
			3.27×10^{-2}	1.05×10^{-1}	0.69	0.49	
Week 5	4.19×10^{-17}	0.54	2.47×10^{-1}	1.00×10^{-11}	0.18	1.00	1.84
			3.97×10^{-2}	9.74×10^{-2}	0.66	0.49	
Week 6	7.59×10^{-17}	0.49	5.26×10^{-1}	1.00×10^{-11}	0.21	0.82	1.69
			7.93×10^{-2}	1.27×10^{-1}	0.49	0.66	
Week 6 Ext	1.44×10^{-17}	1.00	2.10×10^{-1}	8.90×10^{-6}	0.86	0.02	1.79
			2.80×10^{-1}	8.35	0.25	1.00	

4.4.2.2 FTIR Measurements

Heavy oxidation of the UHMWPE was observed within the FTIR spectrum after six weeks of accelerated weathering when compared to the pristine measurements. The wavenumbers 3600-2900 cm^{-1} correspond to the presence of hydrogen bonded hydroxyl groups and C-H bond stretching. However, the values of 1712, and 1300-1176 cm^{-1} correspond to the presence of C=O and C-O bonds, respectively. Both of these peaks were significant and broad, indicating there were a large amount of these bonds present within the polymeric chains.
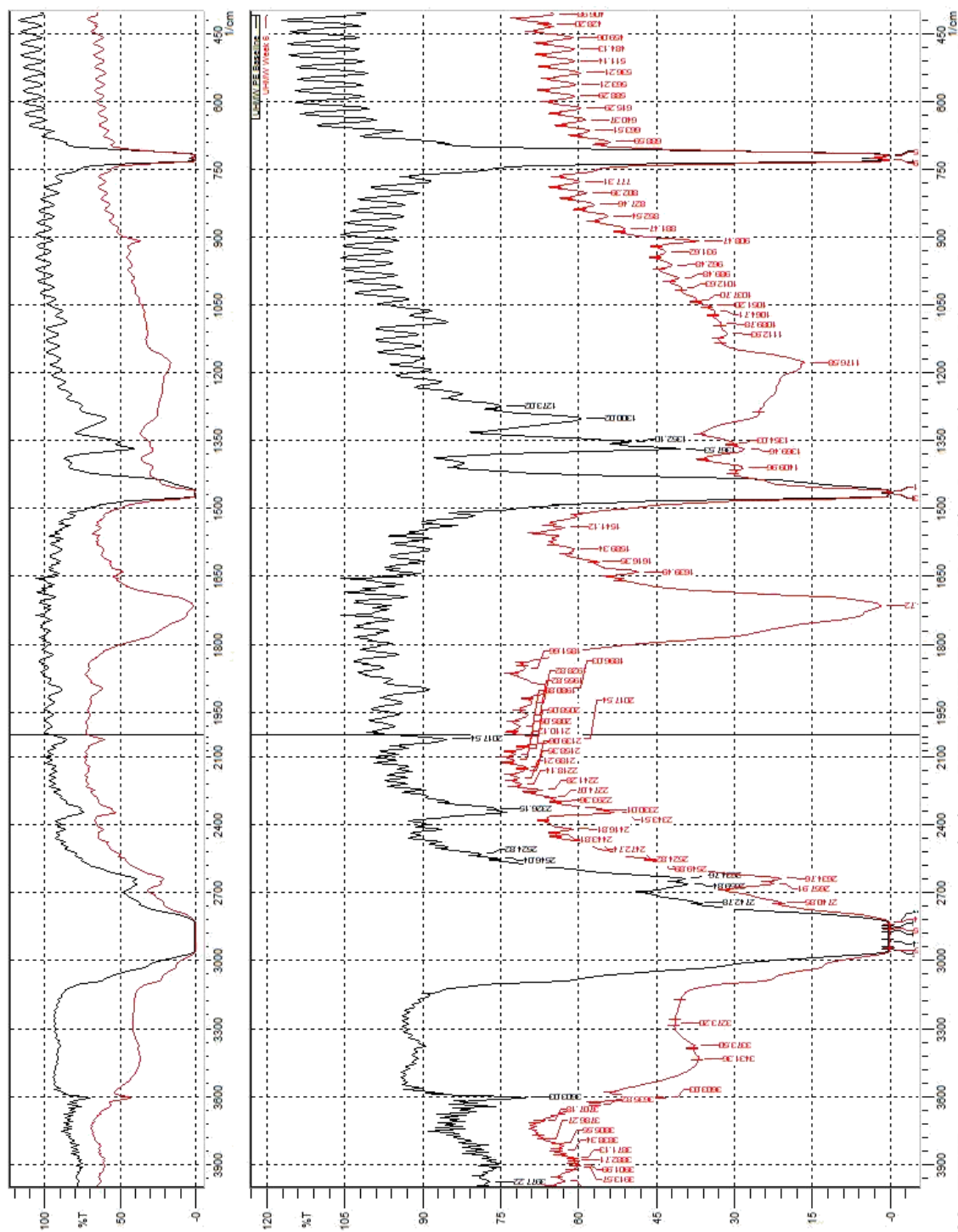
Figure 39. FTIR measurements on a pristine UHMWPE sample (displayed in black) and the sample weathered for six weeks (displayed in red), showing peak formation around 3600-2900, 1712, and 1300-1176 cm^{-1}.

4.4.3 Thermal Degradation Experiment

After a week of thermal aging at 100 °C, ε' and ε'' were observed to increase with time (Figure 40). The values did not increase significantly during the first 24 hours of aging but after one week more noticeable changes were observed. All the measured values were above the variance of the values measured on pristine samples. The real permittivity increased from about 2.14 to about 2.18 during this time. Also, a relaxation around 2.5 Hz appeared and is likely the γ-relaxation caused by the presence of hydroxyl ions (similar results as the weathering experiment).

During thermal aging, in general, all the fit parameters were found to decrease with aging time. The relaxation time for the γ-relaxation is the exception to this trend as the values fluctuated between tests. All the fit parameters are shown in Table 14.
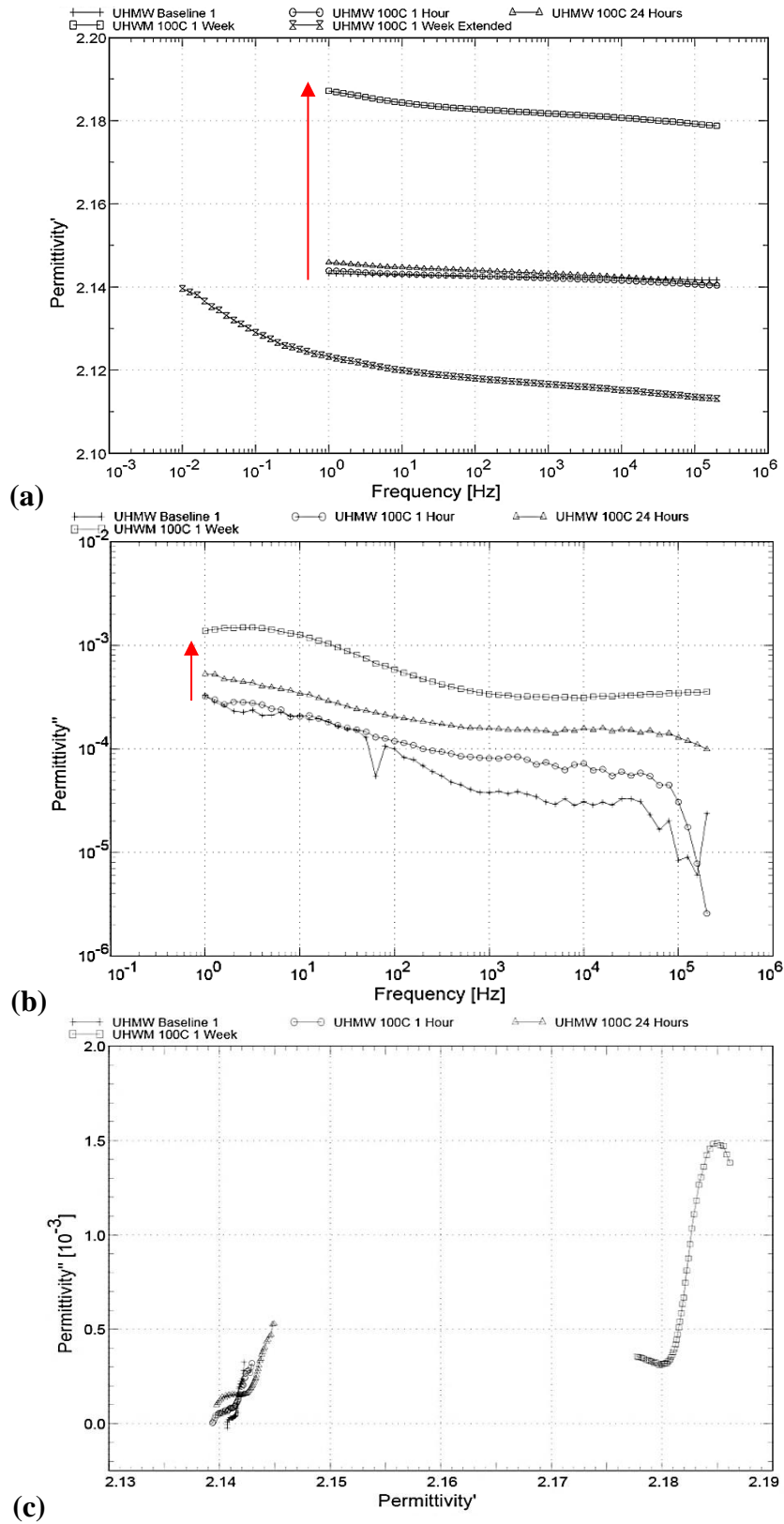
Figure 40. Thermally aged UHMWPE dielectric measurements plotted as ε' versus log (frequency) (a), log (ε'') versus log (frequency) (b) and a Cole-Cole representation (c). The red arrows indicate trends present within the data.

Table 14. Low frequency fit parameters for the thermally aged UHMWPE samples.

Sample	σ (S/m)	S	$\Delta\varepsilon$	τ (s)	α	β	ε_∞
Low 2	$1.00\text{x}10^{-20}$	0.45	$2.69\text{x}10^{-4}$	$1.79\text{x}10^{-2}$	0.93	1.00	2.03
			$8.12\text{x}10^{-4}$	$1.21\text{x}10^{-3}$	0.60	0.20	
Low 3	$1.38\text{x}10^{-16}$	1.00	$5.91\text{x}10^{-4}$	$2.17\text{x}10^{-2}$	0.77	0.76	2.07
			$1.58\text{x}10^{-4}$	$7.62\text{x}10^{-3}$	0.90	0.17	
1 Hour	$5.24\text{x}10^{-17}$	0.89	$1.30\text{x}10^{-3}$	$1.06\text{x}10^{-1}$	0.74	0.50	2.09
			$1.03\text{x}10^{-3}$	$8.53\text{x}10^{-6}$	0.34	0.78	
24 Hours	$3.71\text{x}10^{-19}$	0.60	$4.65\text{x}10^{-3}$	$5.26\text{x}10^{-2}$	0.63	1.00	1.94
			$2.68\text{x}10^{-1}$	$7.49\text{x}10^{-7}$	0.13	0.01	
1 Week	$1.00\text{x}10^{-20}$	0.56	$6.76\text{x}10^{-3}$	$8.65\text{x}10^{-2}$	0.48	1.00	1.84
			$5.78\text{x}10^{-1}$	$7.05\text{x}10^{-10}$	0.26	0.01	

CHAPTER 5. DISCUSSION OF RESULTS

Each of the materials examined exhibited a strong tendency to oxidize as a result of the accelerated weathering process. This oxidation had different effects on each material's dielectric properties due to their differences in chemical species but similar results were obtained. The typical chemical species formed due to oxidation were hydroxyl and carbonyl groups. These groups had the general effect of causing the characteristic relaxation frequencies to decrease and cause an increase in ε' with a larger degree of changes being observed than those of the thermally aged samples.

EVOH has two characteristic relaxations which occur within the frequency range being examined here, a MWS relaxation and a β-relaxation. The cause of the MWS relaxation is addressed in the previous chapters but the β-relaxation has been suggested to likely be caused by the local relaxation of crystalline regions or the movement of hydroxyl groups which may interact with each other from one vinyl alcohol groups to another, inhibiting chain motion [6]. Despite having heavy oxidation and the samples being physically destroyed (shown in Figure 17) as a result of the accelerated weathering, no significant changes in the β-relaxation were observed; however, the thermally aged samples showed a decrease in this relaxation frequency. This could be the result of increased cross-linking or chain entanglement due to the increased amount of hydroxyl group interactions with the vinyl alcohol groups. Similar results were obtained in terms of the MWS relaxation but in the opposite way. With increased thermal aging time, the relaxation became more prominent within the spectrum and shifter to higher frequencies. This effect likely indicates that there was an increase in interfaces as a result of the polymer being held near its melting point for

the extended amount of time in air and that the charges along the interfaces had more mobility.

PEEK, similarly to EVOH, has two relaxations within the frequency range studied which influence its dielectric response, a β-relaxation and a MWS relaxation. The β-relaxation is characterized by the localized non-cooperative motions of the chain fragments, primarily the rotation of the aromatic rings [12]. These two relaxations were observed to have their characteristic relaxation frequency decrease with increased accelerated weathering and thermal aging. These results agree with the published results found during the literature review pertaining to radiation exposure and thermal aging (described in Chapter 2) [9, 10]. These decreases are likely the result of increased cross-linking and oxidation which inhibit the mobility of the aromatic rings. The values of the real permittivity were also found to increase with increased aging, which also agrees with information available in the literature [11].

Within the frequency range examined here, PPS has two relaxations (MWS and β_{II}-relaxations) which contribute significantly to the spectrum and another, which only has a slight influence (β_I-relaxation) until higher frequencies. The β_{II}-relaxation is associated with the resonance of the aromatic ring while the β_I-relaxation is due to the movement of the stiff chains [13, 15]. After accelerated weathering and thermal aging, the relaxation frequency of the β_{II}-relaxation was observed to decrease for both experiments. This is due to oxidation of the aromatic rings and the sulfur atoms and cross-linking/crystallization because the relatively simple structure was replaced with more bulky groups which became more tightly bound together, decreasing the mobility of the aromatic rings.

UHMWPE has two possible low frequency relaxations, a γ-relaxation and a β-

relaxation, which has a small effect on the measurements of the pristine samples. As weathering and thermal exposure increased the two relaxations shifted to lower frequency. The β-relaxation also became a more prominent feature within the dielectric spectra. This relaxation is characterized by the movement of defects within the normal structure which can include chain fragment, free radicals and alterations in the chemical structure.

Finally, it should be noted that once the polymers were thermally aged near their melting point, the shrinkage and stiffening observed could partially be attributed to the burning off of any leftover products from processing (i.e. catalysts, plasticizers, stabilizers, surfactants, etc.) if they were present in the as-received material.

CHAPTER 6. SUMMARY AND CONCLUSIONS

It was found that oxidation, as a result of the accelerated weathering and thermal aging experiments performed on the materials, was the main influence on the observed modifications to the dielectric spectra and associated relaxations of EVOH, PEEK, PPS and UHMWPE. Material changes produced statistically significant increases in permittivity values for weathered samples of PEEK and PPS and thermally-aged samples of EVOH, PEEK, and UHMWPE, whose general trends agree with the reviewed literature. Also, changes within the characteristic relaxation frequencies and fit parameters were observed for each material. These observed alterations in the fitted parameters of the HN model used in the analysis of each material were noted and can serve as a reference for future capacitive measurements to determine if the materials have undergone degradation due to environmental exposure.

REFERENCES

[1]   S. O. Kasap, Principles of Electronic Materials and Devices, Third ed., McGraw-Hill, 2006, pp. 583-673.

[2]   M. Wubbenhorst and J. van Turnhout, "Analysis of complex dielectric spectra. I. One-dimensional derivative techniques and three-dimensional modelling," *Journal of Non-Crystalline Solids,* no. 305, p. 40–49, 2002.

[3]   Novocontrol Technologies, *Novocontrol User Manual,* 2006.

[4]   "John F. Kennedy Space Center FAQ," NASA, 17 11 2000. [Online]. Available: http://science.ksc.nasa.gov/pao/faq/faqanswers.htm. [Accessed 2014].

[5]   D. J. Carlsson, S. Chmela and D. M. Wiles, "The oxidative degradation of ethylene/vinyl alcohol copolymers," *Polymer Degradation and Stability,* vol. 31, no. 3, pp. 255-267, 1991.

[6]   A. Bizet, N. Nakamura, Y. Teramoto and T. Hatakeyama, "The influence of moisture on the dielectric properties of poly(ethylene-co-vinyl alcohol)," *Thermochimica Acta,* vol. 241, pp. 191-198, 1994.

[7]   Victrex, "Victrex PEEK Properties Guide," 2014.

[8]   W. K. Sakamoto, "Dielectric spectroscopy and thermally stimulated discharge current in PEEK film," *Ecletica Quimica,* vol. 28, no. 2, pp. 49-53, 2003.

[9]   "Influence of Crystallinity on the Dielectric Relaxation Behavior of Poly(ether ether ketone)," *Macromolecules,* vol. 26, pp. 4252-4261, 1993.

[10] M. Arous, I. B. Amor, A. Kallel, Z. Fakhfakh and G. Perrier, "Crystallinity and dielectric relaxations in semi-crystalline poly(ether ether ketone)," *Journal of Physics and Chemistry of Solids,* vol. 68, pp. 1405-1414, 2007.

[11] K. Y. Kim, C. Lee, P. J. Kim and B. H. Ryu, "Dielectric Properties on the Radiation and Thermal Aged PEEK," in *2004 International Conference on Solid Dielectrics*, Toulouse, 2004.

[12] A. Leonardi, E. Dantras, J. Dandurand and C. Lacabanne, "Dielectric relaxations in PEEK by combined dynamic dielectric spectroscopy and thermally stimulated current," *J. Therm. Analytical Calorimetry,* vol. 111, pp. 807-814, 2012.

[13] "Dielectric Properties of Polyethylene Terephthalate/Polyphenylene Sulfide/Barium Titanate Nanocomposite for Application in Electronic Industry," *POLYMER ENGINEERING AND SCIENCE,* pp. 1613-1619, 2010.

[14] F. F. Fondeur, D. T. Herman, M. R. Poirier and S. D. Fink, "The Chemical and Radiation Resistance of Polyphenylene Sulfide as Encountered in the Modular Caustic Side Solvent Extraction Processes," Aiken, 2011.

[15] P. Huo and P. Cebe, "Dielectric Relaxation of Poly (Phenylene Sulfide) Containing a Fraction of Rigid Amorphous Phase," *Journal of Polymer Science: Part B: Polymer Physics,* vol. 30, pp. 239-250, 1992.

[16] S. Yasufuku and M. Todoki, "Dielectric and thermoanalytical Behaviors of Poly(p-phenylene Sulfide) Polymers," in *Conference Record of the 1992 IEEE International Symposium on Electrical Insulation*, Baltimore, 1992.

[17] R. D. Mathad, H. H. Kumar, B. Sannakki, G. Sanjeev, K. Sarma and S. Francis, "Electron-beam-induced changes in ultra-high-molecular weight polyethylene," *Radiation Effects & Defects in Solids: Incorporating Plasma Science & Plasma Technology,* vol. 165, no. 4, pp. 277-289, 2010.

[18] C. S. Brazel and S. L. Rosen, Fundamental Principles of Polymeric Materials, 3rd ed., Wiley, 2012.

[19] *ASTM Standard G155,* West Conshohocken, PA: ASTM International, 2013.

[20] Iowa State University Deparment of Material Science and Engineering, "Shimadzu FTIR Standard Operating Procedure," 2014.

[21] *ASTM Standard D3045,* West Conshohocken, PA: ASTM International, 2010.

[22] Kuraray, "EVAL EVOH Resins," 2014.

[23] Chevron Phillips Chemical Company, "Ryton PPS Data Sheets," 2014.

[24] R. M. Silverstein, F. X. Webster and D. J. Kiemle, Spectrometric Identification of Organic Compounds, Seventh ed., Hoboken, New Jersey: John Wiley and Sons, 2005.